Modified nanodiamond particle size studies by means of dynamic light scattering technique

Field of study: Electronics and Telecommunications

Specialization: Computer Electronic Systems Engineering

Author: Efosa Ojomo

Supervised by: dr hab. inż. Robert Bogdanowicz

ABSTRACT

The Methods Utilizing the Phenomena of Light Scattering to Measure Particle Size distribution in different solvent, such as deionise water and alcohol and also to study the various structural formation when nanodiamond solution is placed on silicon surface.

The purpose of this research project is divided into two parts

1. to configure the measurement units for examining modified nanodiamond particles, examination of their sizes when placed in different solvents and observing the zeta potential of the particles when placed in different solvents.
2. to observe the structural formation for different nanodiamond particles droplets on silicon glass.

The particle size distribution will be measured using dynamic light scattering techniques using derived solutions made from either deionized water or alcohol. The particle charges will be determined using the zeta potential.

The structural formation drawn by droplets of nanodiamond particles will be observed using a biological microscope.

Table of Contents

List of abbreviations

Highly Oriented Pyrolytic Graphite (HOPG)

The Autocorrelation Function (ACF)

Dynamic Light Scattering (DLS)

Rotation per minute (RPM)

High Pressure and Temperature (HTHP)

Chemical vapour deposition (CVD)

Nano Diamond (ND)

Denotation Nano Diamond (DND)

Quasi Elastic Light Scattering (QELS)

Tungsten Carbide (WC)

Rotation Per Minute (RPM)

Bead Assisted Sonic Disintegration (BASD)

Diffusion coefficient (D)

Boltzmann constant (K_B)

Temperature (T)

Viscosity (η)

Chapter 1: INTRODUCTION

1.1 History of Diamond

The only element in the periodic table with four isomers is Carbon, ranging in size from 0 to 3. Graphite with sp2 hybridized bonds and diamond with sp3 hybridized bonds are the two most well-known polytypes. Several "new" carbon forms have gotten a lot of attention in the last 30 years, and they're all variants on the two types of carbon mentioned above. CVD diamond, fullerenes, carbon nanotubes, and graphene are examples of "new" carbon forms. (Stachel, 2014).

Harold W. Kroto, Robert F. Curl, and Richard E. Smalley discovered fullerenes in molecular beam experiments in 1985. C60 is the most prevalent fullerene. It shows a hollow spherical cluster of 60 carbon atoms that makes up a whole molecule. 12 pentagons associated with sp3 hybridization and 20 hexagonal formation of carbon atoms associated with sp2 hybridization combined to form a complete spherical shape in each molecule. (Stachel, 2014).

Carbon nanotubes received a lot of attention when they were first discovered in 1991 because they are one-dimensional nanostructured pure carbon materials with a number of desirable properties important to both industrial applications and basic research. The most recent of the innovative carbon materials is graphene, a one-atom thick layer of two-dimensional carbon atoms with sp2 bonding. According to theory, a single layer graphene sheet should be thermodynamically unstable, however this was refuted in 2004, when it was first produced by physically cleaving Highly Oriented Pyrolytic Graphite (HOPG). (Thandavan, 2010).

Diamond is a cubic high-pressure phase of elemental carbon with a unique Mohs hardness of 10 and perfect octahedral cleavage, as well as a very high density (3.51 g/cm3), refractive index (2.417), dispersion (0.044), and thermal conductivity. At the same time, diamonds are the most valuable and sought-after stones in history. In recent times, the diamond's extraordinary durability, its genesis deep in the Earth's interior (>105 km) and during Earth's early history, as well as innovative advertising, such as the concept "a diamond is everlasting," have all contributed to its elevated prestige. Until the discovery of diamonds in Brazil, India was the world's exclusive provider of diamonds for at least two thousand years (1725) (Thomas Stachel, 2014). Diamonds from Borneo's alluvial Kalimantan fields have most certainly been mined since the 7th century, but have only been traded locally or incorporated into Indian manufacturing until

being transferred to Europe [Ogden 2005]. Following additional discoveries in South Africa (from 1866 onwards), it was eventually realized that diamonds are brought to the Earth's surface in volcanic rocks called "kimberlite" after the town of Kimberley, where the new diamond-bearing rock was first discovered. (Stachel, 2014)

Diamond has evolved into a valuable mineral resource, with yearly output exceeding 124 million carats in 2011, worth US$14.4 billion. Russia, Botswana, the Democratic Republic of the Congo, Canada, Zimbabwe, Angola, South Africa, and Australia are the top diamond-producing countries in terms of carats extracted (Fig. 1.1). (Shantanu, 2015). The diversity of carat price based on production quality separates diamonds from non-gem mineral resources; end-members in the extreme volatility around an average production price of US$ 116 per carat range from US$ 9 (Democratic Republic of the Congo) to US$ 1602 per carat (Kingdom of Lesotho) (Shantanu, 2015). Botswana is the world's biggest diamond producer, followed by Russia, Canada, South Africa, and Angola, based on output value in 2011. (Fig. 1.1). Despite the fact that only roughly a quarter of all diamonds produced are of gem quality, retail sales of diamond jewellery surpass US$ 70 billion. (Stachel, 2014)

Diamond is also the subject of extensive research due to its chemical inertness, deep origin, and creation that dates back to the Paleoarchean period. The majority of this research focuses on minute mineral inclusions that diamond acquired during development and then guarded from chemical modification through later mantle storage and exhumation from depth. These inclusions, as well as the phase assemblages they sample, are the sole clean samples of the deep mantle, and they also reveal information on diamond's origin. Early analytical work (e.g., Mitchell & Giardini 1953) was limited to X-ray diffraction studies due to the small size of diamond inclusions (typically less than 0.02 mm). (Stachel, 2014)

Harris was the first to define visual criteria for identifying mineral inclusions in diamonds (1968a, 1968b). Chemical analysis of inclusions became possible with the development of the electron probe micro-analyzer in the 1960s, and early pioneering work was done at the Carnegie Institution in Washington (Meyer 1968, Meyer & Boyd 1969) and the Russian Academy of Science in Novosibirsk (Sobolev 1970).

Meyer & Boyd (1972), Sobolev (1977), Meyer (1987), and Gurney (1992) provided seminal appraisals of early diamond inclusion studies (1989). These and later research on mineral inclusions in diamonds have altered our understanding of the geochemical and mineralogical environment in which diamonds develop in the Earth's mantle, laying the framework

for a current interpretation of indicator mineral analyses during diamond exploration. (Stachel, 2014)

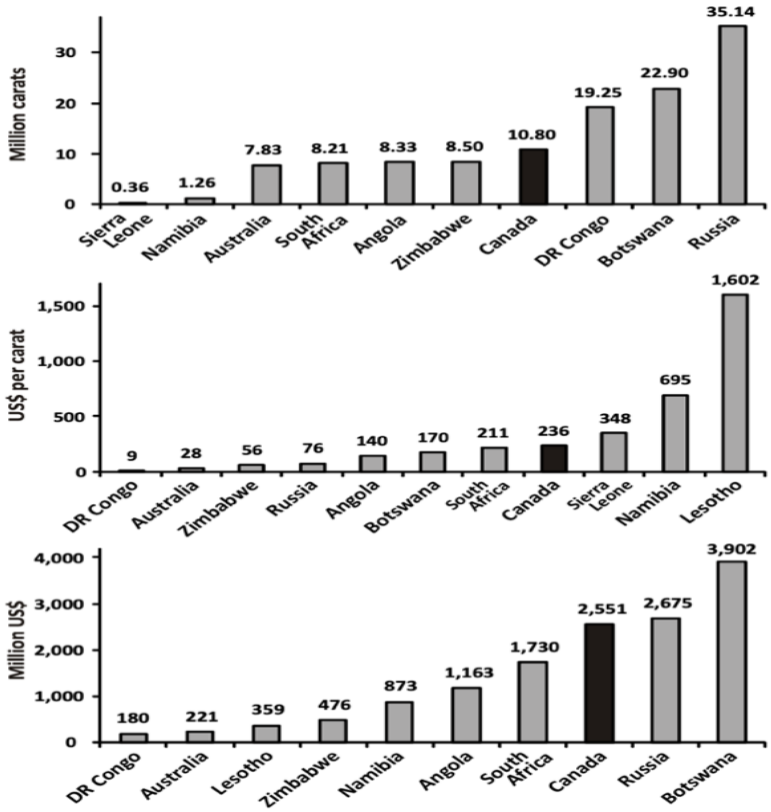

Figure 1.1 Chart of diamond producing countries in the world. (Stachel, 2014)

Figure 1.1 The top 10 diamond-producing countries in the world, measured in million carats extracted. In the middle, the average production price (in US dollars per carat) for a few countries is shown. Bottom: the 10 most valuable diamond-producing countries in the world (in millions of US dollars). Due to an extraordinarily high carat price, the Kingdom of Lesotho, which ranks #14 in production measured by weight, leaps to #8 in production assessed by value. Rough diamond production figures for 2011 from the Kimberley Process (https://kimberleyprocessstatistics.org/public statistics). (Stachel, 2014)

1.2. Origin of Diamond

Primary diamond deposits are found in volcanic diatremes ("pipes") and minor subvolcanic intrusions (dykes and sills), as opposed to secondary diamond deposits, which are formed when primary deposits are eroded and diamonds are transported and re-sedimented in rivers and along oceanic coasts. Diamond development is unconnected to the volcanic host rocks in which they form. Instead, magmatism plays a crucial role in the development of primary diamond deposits by sampling diamonds that already exist deep inside the Earth's mantle and transporting them quickly to the surface. (Capdevila, 1999)

This limits the occurrence of primary diamond deposits to a few types of ultramafic magmatic rocks originating beneath the graphite–diamond transition (> 105–135 km, depending on the local geotherm): Group I ("basaltic") kimberlite, Group II ("micaceous") kimberlite (also known as orangeite), and olivine lamproite. Furthermore, volcaniclastic komatiite has been identified as the parent rock for a unique collection of diamonds discovered in Dachine, French Guiana (Capdevila, 1999)

Boyd & Gurney (1986) and Haggerty (1986) linked the observed close association between diamondiferous kimberlite and Archean cratons (known as "Clifford's Rule," as revised by Janse 1994) to deep reaching (down to ca. 200 km) and chemically highly depleted lithospheric keels that are generally absent beneath younger crust. Subcratonic lithospheric mantle is colder than convecting asthenospheric mantle at similar depths (e.g., Rudnick & Nyblade 1999), leading the graphite– diamond transition to rise to a shallower depth (see Figure. 1.2). (Stachel, 2014)

A "diamond window" is formed when the lithospheric mantle enters the diamond stability field, with the exact thickness of this window fluctuating across and within cratons dependent on both lithospheric thickness and local geothermal gradient. The need for rapid ascent of magmas from the diamond window, assisted by the brittle character of the lithospheric mantle, to retain diamonds explains why primary diamond deposits are restricted to lithosphere extending into the diamond stability field. (Eggler 1989).

Furthermore, because carbon is a trace element in the Earth's mantle (Trull, 1993), macro-diamond creation necessitates local carbon enrichment, which is thought to be associated to redox fronts. The close link between diamonds and harzburgite/dunite shows that the extremely depleted lithospheric mantle operates as a carbon trap for upwelling fluids or melts

(Gurney, 1984). Recent evidence indicating a reduced character of deep cratonic peridotite (Woodland & Koch 2003, McCammon & Kopylova 2004, Creighton et al. 2009, 2010) is consistent with an oxidized character (i.e., carbonate-bearing) of diamond-precipitating fluids, as proposed by Haggerty (1986). Such oxidized fluids cannot be obtained from the deep convecting upper mantle, which is even more reduced than the cratonic lithosphere (Ballhaus 1992), but could be related to subducting oceanic slab devolatilization. However, the alternate concept, in which methane-bearing asthenospheric fluids are oxidized to water and diamond as they ascend along a gradient of increasing oxygen fugacity, is as conceivable (Taylor & Green 1989), (Huizeng, 2012). Eclogite is the cratonic lithosphere's second most important diamond supply rock. It's been proposed that eclogite and peridotite in the subcratonic lithospheric mantle are reduced in a similar way (Simakov 2006), implying a similar diamond generation mechanism. However, because the mineralogical composition of eclogite prevents restricting silica activity, precise estimations of oxygen fugacity are still missing (an essential parameter for available oxybarometers). (Stachel, 2014)

The convecting mantle (asthenosphere to lower mantle) underlying the common diamond sources in ancient and rigid cratonic lithosphere appears to be generally associated with recycled oceanic lithosphere transporting carbon (as organic matter or carbonate) back into Earth's deep mantle and possibly also providing steep redox gradients (Stachel 2001). The need for quick exhumation appears to limit sublithospheric diamond occurrences to areas with deep-reaching cratonic keels. The presence of micro-diamonds in UHP terranes (e.g., Sobolev & Shatsky 1990, Zhang et al. 1997), the occurrence of graphite pseudomorphs after diamond in peridotite massifs (Pearson et al. 1995), and the common association of nano- to micro-diamonds with astroblemes are all examples of (non-economic) primary diamond occurrences (Carlisle 1991).

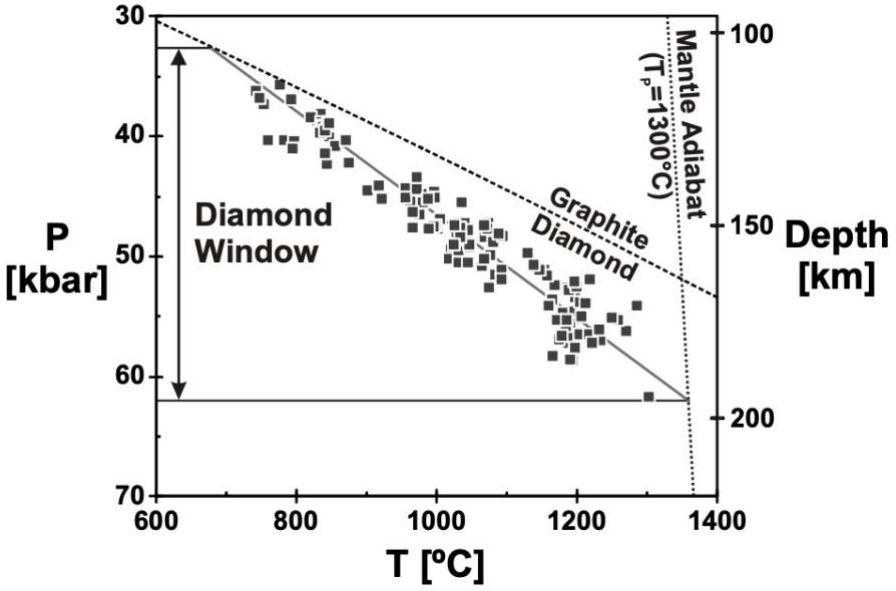

Figure 1.2 Diamond creation and storage in deep-reaching cratonic keels. (Stachel, 2014)

Figure 1.2 shows the conditions of diamond creation and storage in deep-reaching cratonic keels. The single clinopyroxene geothermobarometer of Nimis & Taylor was used to quantify pressure–temperature for garnet lherzolite xenoliths from the middle Slave Craton (Lac de Gras area; Grütter 2009). (2000). A solid grey line represents a linear regression of the data set ("local geotherm"). Day is represented by the graphite–diamond transition (dashed line) (2012). The steeper slope of the revised phase boundary (Day 2012) extends the stability of diamond in Earth's mantle to shallower depths than the graphite–diamond transition proposed by Kennedy & Kennedy (1976), with the difference being especially considerable for places with a "cold" local geotherm (about 30 km difference for the example shown here). Diamond formation and storage conditions in deep-reaching cratonic keels are depicted in Figure 1.2. For garnet lherzolite xenoliths from the middle Slave Craton (Lac de Gras area; Grütter 2009), Nimis & Taylor's single clinopyroxene geothermobarometer was used to quantify pressure–temperature. (2000). The linear regression of the data set is shown by a solid grey line ("local geotherm"). The change from graphite to diamond (dashed line) represents the day (2012). The revised phase boundary's steeper slope (Day 2012) extends diamond stability in Earth's mantle to shallower depths than Kennedy & Kennedy's (1976) graphite–diamond transition, with the difference being notably significant for regions with a "cold" local geotherm. (Stachel, 2014)

1.3. Diamond phase

Humans have admired diamonds since ancient times, mostly as gemstones. It is a status symbol due to its scarcity, hardness, and intense gleam. Apart from being a highly prized jewel, diamond's several outstanding features attract to material scientists and engineers. The hardest known material, chemical inertness, maximum thermal conductivity at room temperature, least compressible, and highest stiffness are among the features. Diamond, when doped, has a higher band gap of 5.4 eV, making it suitable for the production of microelectronic devices for high frequency and high-power applications. (Thandavan 2010).

The valence electrons in carbon are sp3 hybridized to form chemical bonds in diamond, which is carbon in its purest form. Each carbon atom in diamond shares all four of its available electrons with neighbouring carbon atoms, forming a tetrahedral unit with a length of 1.54 A. The strongest known chemical linkage is formed by sp3 hybridized electrons producing the covalent bond, which is responsible for many of diamond's outstanding qualities. (Thandavan 2010)

a b

Figure 1.3 (a) Diamond lattice and (b). Face-centered cubic structure of diamond. Synthesis, Characterization, and Applications of Diamond (Thandavan 2010)

On Figure 1.3, the bond divides each carbon atom into equal angles of $109^{0}28^{0}$. Diamond's recurring structural unit is made up of eight atoms organized in a cube as illustrated in Figure 1.3 (b). (Thandavan 2010)

Diamond crystals can take on a variety of shapes known as 'crystal habits' due to its cubic geometry and highly symmetrical atom arrangement. The most frequent crystal habit is the octahedron. Diamond crystal, on the other hand, can take the shapes of cubes, dodecahedra, and even mixtures of these shapes. Diamond, the ultrahard cubic form of carbon, is a mineral

that requires a long list of superlatives to adequately convey its properties, technological and commercial significance, and historical and cultural significance. The hardest substance known, diamond is a strategic mineral vital to the market in superabrasives, with about 800 million carats (160 metric tons) and a value of around US$109 each year (Olson 2002). With an unrivaled mix of brightness, fire, hardness, and value (US$2 1010 yearly for stones alone) (Olson 2003), diamond, the king of gems, is at the centre of the most lucrative aspect of the gem industry. Natural diamonds are the oldest and most deeply sourced objects we will ever handle, and they provide direct information about the mantle. Diamond's exceptional nature—linking technology, economics, glamour, natural science, and material science—provides a powerful push for ongoing scientific research. As a result, the answer had to be "yes" when asked if diamond could be the first topic for Elements. (Olson 2003).

Table 1. 1 shows the Physical properties of Diamond (George E. and Rondi M., 2005)

Composition	C (carbon)
Crystallographic class	Hexoctahedral – cubic (highest of symmetries)
Common crystal forms {and indices}	111 octahedron, 100 octahedron, 110 octahedron, rounded deviations owing to etching
Hardness	10 on the Mohs scale, 56–115 on the Knoop hardness range, 10,000 on the Brooks indenter scale, octahedral face hardest, cube face softest
Density	3.51 g cm-3 (or 3.51) specific gravity
Colours	Colourless, yellow, blue, green, and a variety of additional colours are available.
Refractive index	2.4175 percent (in the yellow light of a sodium lamp)
Dispersion	The difference in index between G and B Fraunhofer wavelengths is large (0.0437), resulting in rainbow colours on refraction.
Optical transmission	Over a broad range of the electromagnetic spectrum, it is transparent; it is an ideal material for optical windows.
Thermal conductivity	It possesses an excellent thermal conductor, 5 to 25 watts centimeter-1 °C-1 (at 300K); 4 times greater than copper.
Electrical conductivity	It has 0-to-100-ohm cm-1 (300K resistivity); an insulator

In many ways, diamond is a stunning substance. It has a strong rigid framework thanks to its simple but elegant crystal structure (Figure. 1.3), in which each carbon atom is connected to four other atoms in a tetrahedral arrangement. Most of diamond's qualities can be explained by combining this structural arrangement, which corresponds to carbon's hybrid sp3 orbitals, with the unrivalled strength of the C–C bond, as seen in Table 1.1.

Table 1.1 shows the stiff bonding results in a high level of hardness, incompressibility, and heat conductivity. Diamonds are termed "ice" because of their exceptional capacity to transfer heat; they feel freezing cold when your diamond-touched lip loses heat. Diamond is an electrical insulator and transparent over a vast portion of the electro- magnetic spectrum due to its homogeneous covalent bonding, which results in a huge band gap of 5.5 eV. The high refractive index of 2.42, which is rather remarkable for a material with such a low average atomic number, is due to the dense packing of electrons. Diamond's high density (3.51 g cm-3) compared to graphite's (2.20 g cm-3) indicates that it is a high-pressure mineral created largely in Earth's interior. Diamond is a key indicator and recorder of events deep within our planet, in part because of its extreme strength and refractory nature, which allows it to survive exhumation to the surface of the Earth and subsequent weathering. Furthermore, because inclusions captured in a diamond forming in the mantle are preserved by its adamantine embrace, diamonds have become our "space missions" to the interior of the Earth, providing us with the most significant samples for understanding the chemistry of the deep mantle. Researchers have identified the association of diamond with peridotite and eclogite assemblages from the roots of ancient cratons by removing inclusions and analysed them. Signature minerals from the transition zone and lower mantle have recently been discovered. Stachel, Brey, and Harris' contribution examines the current state of these, the deepest samples of Earth we have at our fingertips. While diamonds are essentially pure carbon, isotopic study of C and the minimal N included in them allows us to investigate their carbon origins. Cartigny explains how diamonds reveal the trademarks of ancient Earth, recycled crustal sources, and crystallization processes by presenting the available isotopic data.(George E. and Rondi M., 2005)

Natural polycrystalline diamond carbonado, framesite and microdiamonds discovered in metamorphic rocks over the last 20 years are two less well-known and understood forms of diamond (Heaney, P.J., Vicenzi, E.P., 2005), and examine the properties of carbonado and framesite, attempting to decipher some of the enigma surrounding these intriguing materials. Diamond is a high-pressure mineral that can be used to identify areas of the Earth's crust that have been buried to ultrahigh-pressure (UHP) conditions (for crustal rocks, that is) and then resurfaced with diamonds intact. The search for UHP terranes using diamond or coesite (a high-

pressure form of SiO_2) has become an interesting direction in metamorphic petrology, with significant implications for how the Earth functions. However, tests on the little UHP diamonds themselves have just lately been conducted. Before focusing on the Kokchetav Massif in Kazakhstan, where the most diverse and plentiful microdiamonds have been found (Shimizu, Y., 2003). Ogasawara discusses the UHP occurrences of diamond and the hypotheses behind the methods by which they are generated. (Shimizu, Y., 2003)

1.4 How Diamond Particles are Fabricated

The gem trade has seen synthetic diamond on occasion, but until recently, emphasis was almost entirely focused on the kind formed by subjecting carbon-containing materials to high pressures and temperatures) HTHP (Shigley, 1987). Scientists have known for many years, however, that diamond can be synthesised at low pressures from carbon-containing gases using chemical vapour deposition (CVD) techniques. Although the gem trade has been relatively uninformed of CVD, it has been the topic of considerable international research over the last two decades due to the many possible technical uses of CVD synthetic diamond material.(Martineau, 2004). For the purpose of my thesis, I shall discuss the CVD method of fabricating diamond

1.4.1 CVD Diamond Synthesis

In contrast to the more well-known HPHT-grown synthetic diamond, CVD synthetic diamond is manufactured at low pressures, approximately one-tenth of atmospheric pressure, from carbon-containing gases such as methane (Bachmann,1998). This technique of synthesis includes breaking up gas molecules into reactive species from which diamond may be produced. This may be accomplished in a variety of ways, resulting in a family of related growth strategies.(Martineau, 2004).

The gas molecules (typically methane and hydrogen) are broken apart in a high-temperature plasma created by microwaves in a reactor like the one illustrated schematically in figure 1.4.1. In a recent review, Grotjohn and Asmussen (2002) reported this method—microwave plasmaassisted CVD. Other strategies involving the use of a hot filament, flame, or plasma jet have been examined by Yehoda (2002), Wolden (2002), and Heberlein and Ohtake (2002). (Martineau, 2004).

CVD synthetic diamond is typically formed on a substrate at temperatures ranging from 800–1000°C. Many industrial applications employ silicon or metal substrates, and the material

formed is polycrystalline because several crystals nucleate with distinct crystallographic orientations on the substrate (Wild, 1993). Such substance is incredibly difficult to polish into anything approaching a typical gemstone. (Martineau, 2004).

A single-crystal diamond substrate, on the other hand, can be utilised as a template for continued single-crystal development, in which synthetic diamond develops with the same crystallographic orientation across the substrate. This is known as homoepitaxy. CVD synthetic diamond created in this manner can be polished into faceted stones for jewellery purposes if grown to a sufficient thickness. HPHT diamond synthesis is commonly performed at temperatures and pressures (about 1400°C and 55 kbar) where diamond is the most stable form of carbon. Diamond is metastable under the low-pressure conditions utilised in CVD synthesis. (Martineau, 2004).

This implies that it does not naturally convert to graphite, rather it must be prevented from developing. Standard CVD procedures employ a hydrogen-rich gas combination, and the atomic hydrogen produced in the CVD process plays a significant role in inhibiting graphite production (Butler, 1998).

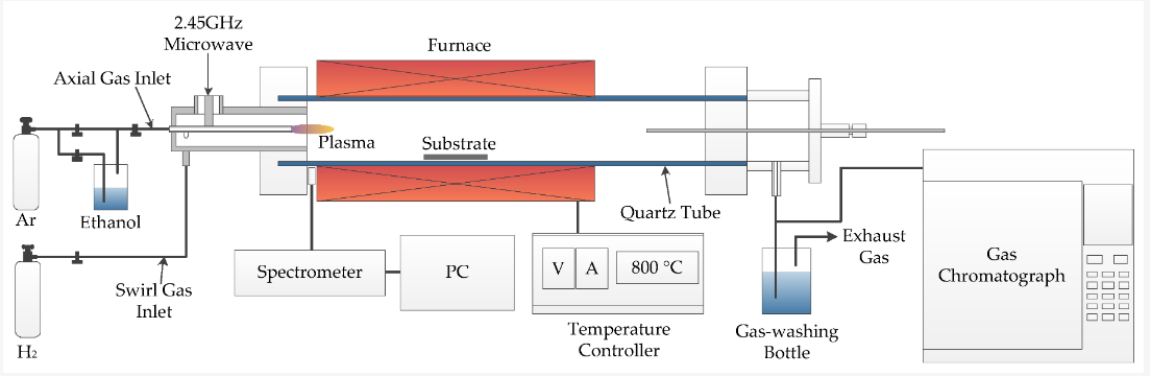

Figure 1.4 Schematic depiction of the air pressure microwave plasma chemical vapour deposition (AMPCVD) method used to synthesise carbon nanotubes (CNTs). (Dashuai, 2020)

This schematic displays a microwave CVD reactor used to create CVD synthetic diamond. The molecules of the initial gases, which are mainly methane and hydrogen, are dissociated in a plasma created by microwaves.

To manufacture CVD diamond material, the chemical species produced react at the surface of seed crystals (substrates) placed at the reactor's base. The diameter of the acceptable growing region might vary between 2 and 20 cm.

1.5 Modified Nanodiamond Particle Size

The sizes of diamond can vary from different nm based on the modification it has undergone. Nanoparticle surface modification refers to the physical and chemical deep processing of nanoparticle surfaces in order to manage internal stress, increase the repulsive force between nanoparticles, and reduce the gravitational attraction between the particles. (George E. and Rondi M. 2005)

The fourth state of matter refers to the size of a substance after it has been micro nanosized, especially in the nano-state, when it is between atoms, molecules, and bulk materials. Because nanoparticles have so many unique features, nanomaterials research has sparked a lot of interest. They've created a wide range of nano- and nano-composites with sophisticated features and high performance that are widely used in a variety of fields. Surface atoms are very active, exceedingly unstable, and easy to agglomerate due to their tiny particle size, huge specific surface area, poor atomic coordination, and high surface energy of nanoparticles. The nano-effects of these agglomerated secondary particles are difficult to achieve, making the material less than optimal. As a result, surface modification of nanoparticles is necessary to improve nanoparticle dispersibility in a polymer mixture system and increase the binding force of nanoparticles to other components. Physical and chemical properties of the nanoparticle's surface (morphology, crystal structure, defect state, stress state, functional group surface energy, surface hydrophobicity, surface wettability, surface potential, surface adsorption and reaction characteristics, etc.) are purposefully changed to give the nanoparticle a new function and meet the needs of nanoparticle processing and application. (George E. and Rondi M. 2005)

1.5.1 Nanoparticle Agglomeration: What Causes It?

This is because there are no nearby coordination atoms, the nano-action energy is an intrinsic characteristic of the nanoparticle's surface, and the intrinsic properties of the nanoparticles are agglomerated with each other. The adsorption force of a nanoparticle with a unit specific surface area should be the physical meaning. (George E. and Rondi M. 2005)

It is the total of numerous elements of nanoparticle adsorption: hydrogen bonding between nanoparticles, electrostatic adsorption; quantum tunnelling between nanoparticles, charge transfer, and localized adsorption of interface atoms; large specific surface of nanoparticles Adsorption. The ability of nanoparticles to aggregate is aided by the nano-effect energy. The nano-action energy must be attenuated or reduced to create nanoparticles with high dispersion, tiny particle size, and narrow particle size distribution. It is the total of numerous elements of nanoparticle adsorption: hydrogen bonding between nanoparticles, electrostatic adsorption; quantum tunnelling between nanoparticles, charge transfer, and localized adsorption of interface atoms; large specific surface of nanoparticles. Adsorption. The facile aggregation of nanoparticles is aided by the nano-effect energy. The nano-action energy must be lowered or reduced to obtain nanoparticles with excellent dispersibility, tiny particle size, and narrow particle size distribution.

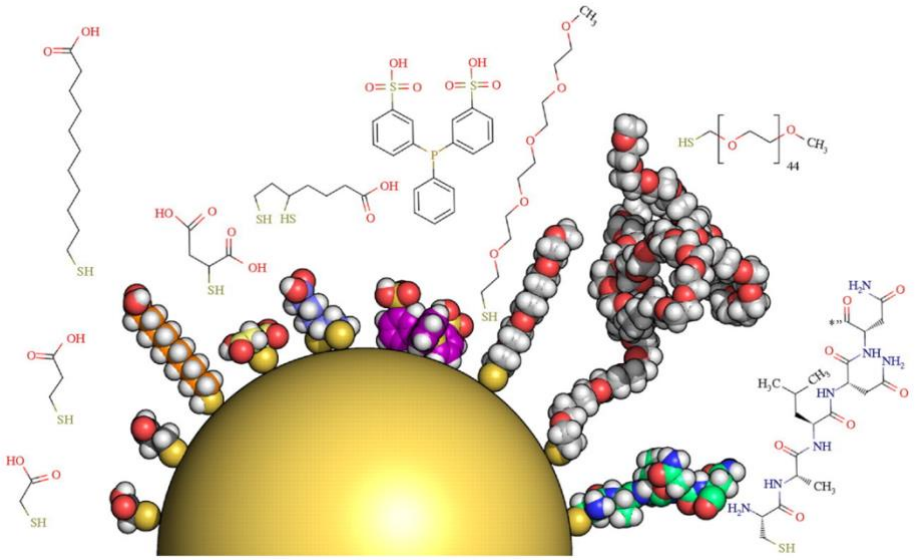

Figure 1. 5 The surface modification of nanoparticles is depicted graphically. (George E. and Rondi M. 2005)

1.6 Surface Modification of Nanoparticles

Depending on the treatment approach chosen, existing methods for surface modification of nanoparticles can be classed as physical modification or chemical modification. .(George E. and Rondi M., 2005)

Surface physical modification refers to a method of surface modification of micro/nano powders without the use of surface modifiers, such as electromagnetic wave treatment, neutron fluxes, alpha particles, beta particles, and sonication, as well as plasma treatment, heat treatment, Electrochemical treatment, and other methods. (George E. and Rondi M., 2005)

1.6.1. Radiation Therapy

Radiation technology is a new field of study that focuses on the principles of physics, chemistry, and biological impacts induced by the interaction of ionizing radiation with matter. High-energy irradiation creates active patches on the surface of the nanoparticle, and the active organic monomer is grafted on the surface of the polymer film to alter the surface properties of the micro-nano particles and improve compatibility with the polymer material. (George E. and Rondi M., 2005)

1.6.2. Treatment with Ultrasonic waves

Ultrasonic dispersion is an excellent approach for reducing nanoparticle aggregation. The nano-effect energy between nanoparticles can be decreased to a great extent by utilizing local high temperature, high pressure, or a powerful shock wave and micro jet generated during ultrasonic cavitation, and nano-particle agglomeration can be effectively prevented. Also, make it completely distributed. (George E. and Rondi M., 2005)

1.6.3. Treatment with Plasma

Plasma treatment has the following advantages: Only a thin layer on the surface of the nanoparticle changes, while other characteristics such as particle size and distribution do not change significantly; the process uses very little energy, and the entire process does not require a solvent; the properties of the polymer, such as functional groups, reactivity, and so on, may vary depending on the application. The downside of this treatment procedure, however, is that it must be performed under vacuum. (George E. and Rondi M., 2005)

1.6.4. Chemical alteration of the surface

Surface chemical modification is a technique for altering the structure and state of a nanoparticle's surface by a chemical reaction or chemisorption between the nanoparticle's surface and the treatment agent. When it comes to surface modification of nanoparticles, the surface chemical modification process is particularly essential. It includes the esterification reaction technique, surfactant method, coupling agent method, and surface graft reaction method, among others. (George E. and Rondi M., 2005)

1.6.5. Method of Esterification

Esterification is the chemical reaction between metal oxides and alcohols. The most significant feature of esterifying nanoparticle surfaces is changing the original hydrophilic and oleophobic surface to a lipophilic and hydrophobic surface. In practical applications, it is critical. (George E. and Rondi M., 2005)

1.6.6. Method of Surfactant Modification

Surfactant molecules are made up of two unique components: an oleophilic group that has an attraction for oil or organic materials, and a hydrophilic group that has an affinity for water or an inorganic substance. The surfactant's structural properties allow it to be used in the surface modification of nanoparticles, converting the hydrophilic groups on their surfaces to oleophilic groups, enhancing the nanoparticles' attraction for organic compounds, as well as their compatibility and dispersibility. (George E. and Rondi M., 2005)

1.6.7. Method of a Coupling Agent

The coupling agent is an amphoteric chemical compound that is mostly employed as an auxiliary agent for polymer polymers. A portion of the group in the molecule can create a strong chemical connection with various functional groups on the powder's surface, while another portion of the group can undergo some chemical reaction or physical entanglement with the organic polymer. As a result, the coupling agent is referred to as a "molecular bridge" since it improves the interfacial contact between the inorganic and organic substances, so considerably increasing the composite material's performance. Silane coupling agents, titanate coupling agents, zirconium aluminate coupling agents, aluminate coupling agents, and others are often used coupling agents. (George E. and Rondi M., 2005)

1.6.8. Surface Graft Modification

A chemical reaction bonds a polymer substance to the surface of an inorganic particle in the process known as surface graft polymerization. Some of the hydroxy or unsaturated bonds found on the surface of some inorganic particles (such as SiO_2, TiO_2, Al_2O_3, carbon black) can be utilized directly to graft the polymer, or the hydroxyl group can be chemically reacted before grafting. Grafting polymer molecules on the surface of nanoparticles offers a higher advantage than utilizing surfactants or coupling agents in that it increases nanoparticle dispersion stability as well as resin matrix compatibility. By choosing appropriate grafting monomers and grafting circumstances, the polymer grafted particles will have tuneable characteristics. (George E. and Rondi M., 2005)

The surface modification of nanoparticles is closely connected to the application of nanoparticles due to their aggregation. There are various methods for surface modification already available, but there are still few approaches to tackle the problem fundamentally, necessitating future study. In addition, in order to produce greater surface modification effects, the composite usage of modifiers should be explored in nanoparticle surface modification. (George E. and Rondi M., 2005)

Chapter 2: METHODS

2.1 Overview of Light Scattering Techniques

My main focus in this thesis will be on Dynamic Light Scattering (DLS) approaches for nano particle manipulation. But, before I go any further, I'd like to briefly explain Light Scattering as a mechanism for particle size change. (Lars, 2019)

The sky is blue because particles scatter light, which is a basic reality that we all experience on a daily basis. This is because blue light is scattered more easily by air particles than red light. The surface particles decide whether the surface is glossy. Materials' size, charge, and molecular weight can be calculated by measuring the angle of light scattering, frequency of light scattering, and intensity of light scattering. (Lars, 2019)

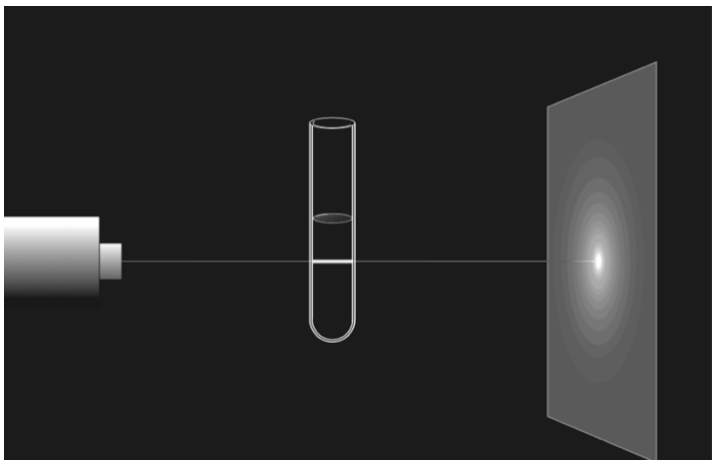

Figure 2.1 depicts light passing through a still water and its reflection on a plane surface (Lars, 2019)

2.2 What is light scattering and how does it work?

Light scattering is what happens when light "hits" a small object (a particle or a molecule) and alters its direction as a result. If, on the other hand, light is absorbed when it comes into contact with a particle, the occurrence is known as absorption. (Lars, 2019). In essence, light interacts with matter in two ways, much like all other types of electromagnetic radiation (radio

waves, micro waves, thermal radiation, ultraviolet radiation, X-rays, and gamma radiation). (Lars, 2019)

1. Absorption: the photons (light) are absorbed.

2. Dispersion (scattering that occurs when photons shift direction

In this section, I'll only discuss dispersion. And just scattering from randomly positioned (and moving) particles spread in a liquid. When light is scattered by ordered particles, phenomena such as reflection, refraction, and diffraction can occur. When a light beam passes through a solution1 of particles, both of the foregoing interactions lead it to be attenuated (see figure 2.0.1). Whether light is dimmed by scattering or absorption, the result is the same: In both circumstances, the transmitted intensity decreases exponentially as the thickness of the substance through which the light passes decreases. The transmitted intensity I is commonly expressed if the attenuation is due to absorption**.** (Lars, 2019)

$I = I0 \cdot 10^{-\alpha x}$ Equation 2. 1 (Lars, 2019)

whereas if the attenuation is due to scattering the intensity is written

$I = I0 \cdot e^{-\tau x}$ Equation 2. 2 (Lars, 2019)

where I0 denotes the intensity of the occurrence (i.e Before attenuation). The absorption coefficient and the turbidity are the two numbers, respectively. The two different bases for exponential decays (e and 10) are just a matter of convention. When undertaking light scattering measurements in the domains of physics or chemistry, the system under observation is almost often a solution of molecules. (Lars, 2019)

But what does the phenomena of light scattering look like in real life? Consider the following examples:

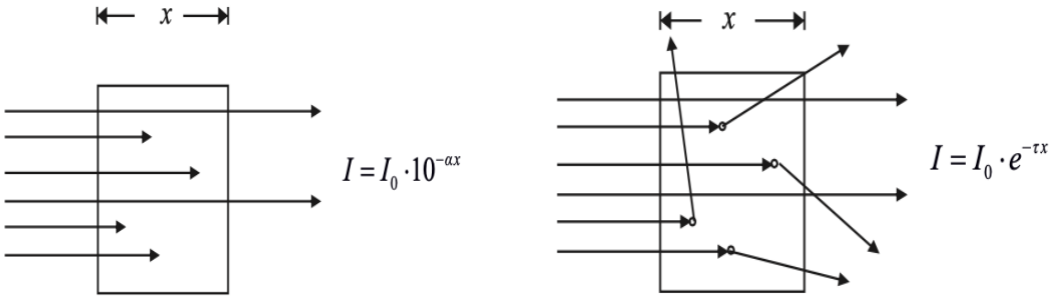

Figure 2.2 Absorption (top) or scattering (bottom) diminish the transmitted light (bottom). (Lars, 2019)

Figure 2.3 laser turned off in a dark environment (Lars, 2019)

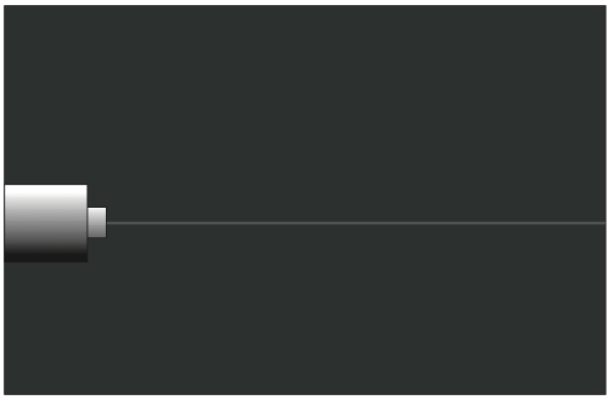

Figure 2.4 laser turned on in a dark environment. The laser beam is almost imperceptible. (Lars, 2019)

In the dim light, the laser beam may be seen. But why is that? To perceive an item, it must be struck by light, which then bounces off in various directions, including into our eyes. By gathering the light reflected from the item, the lens in the eye creates a picture of the thing on the retina. A laser beam, on the other hand, is neither an object nor a "thing." I is just the word for a train of photons travelling in the same direction inside a small area of space. So how come we

can see he laser beam? We are unable to do so. At least not if the laser beam is emitted in a room with completely pure air, i.e. no dust. We observe photons dispersed on dust particles along the course of a laser beam when we look at it (see Figure 2.5).

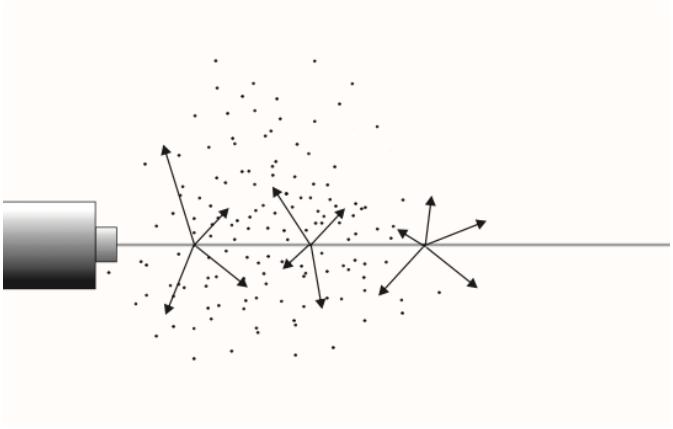

Figure 2.5 light beam (Lars, 2019)

As seen in Figure 2.4. a light beam is not a physical thing, Objects may be seen when they emit light into our eyes, either by emitting light themselves or by reflecting or scattering light that falls on them. A laser beam is a collection of photons moving in the same direction in a controlled manner inside a small area of space. The laser beam is visible from the side because some photons collide with dust particles in the air and are reflected into our eyes.(Lars, 2019)

The simple reason for why we observe an illuminated area when the laser beam impacts a screen or a wall is because of the solid surface. We won't see a bright area where the laser beam impacts if the screen is replaced by a mirror or a glossy surface: Because all of the photons are dispersed (or, in this case, reflected) in the same direction, it's doubtful that any of them will reach our eyes. (See Figure 2.5) Even if the liquid seems perfectly clear and transparent to the eye, a test tube (or even better, a light scattering cuvette) filled with skim milk diluted 1000 times under the laser beam would look like Figure 2.7.

Figure 2.6 laser switched on in a dark environment (Lars, 2019)

In a dark environment, the laser is switched on. A small portion of the screen is illuminated by the laser beam, which appears as a brilliant spot. Because photons are dispersed in all directions from the surface, the region where the laser beam reaches the screen is visible. This necessitates a matte, or sufficiently abrasive, surface.

There is no bright spot when the screen is replaced with an extremely smooth, polished surface, such as a mirror. The reason for this is that the smooth surface does not scatter photons in all directions, but just in one, which is most likely not straight into our eye (s).

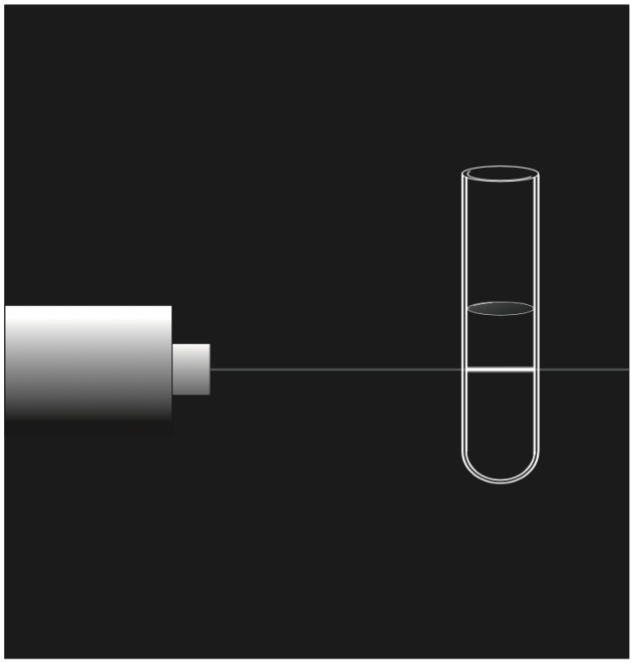

Figure 2.7 laser beam travelling through a solution of particles.

This produces a luminous line in the solution The light is scattered by the particles (or molecules) in this case. The more particles there are and the higher the concentration, the brighter the glow will be.

Polymers with a sufficiently high molecular weight, such as proteins or polysaccharides, are generally polymers of biological origin. These biological polymers are large groups of molecules with molecular weights ranging from around 1000 g/mol to over one million g/mol. The lower the molecular weight, the less dissolved material is required to generate a particular intensity of light scattering. The dispersion will appear like Figure 2.7 if a thin solution of ordinary milk (not skim milk) is placed in the test tube**.** Light dispersion occurs when light on the screen is not limited to a tiny, bright point. (Lars, 2019)

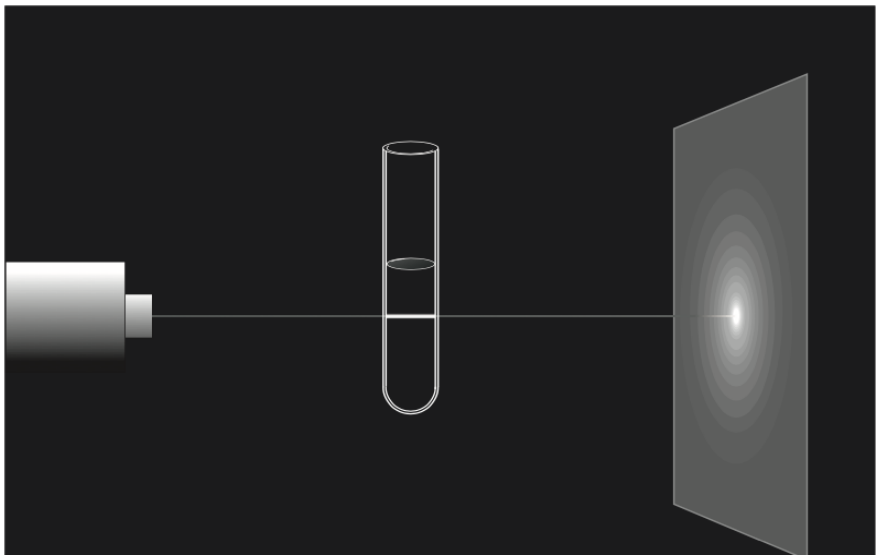

Figure 2.8 A screen behind a solution of light-scattering molecules

This shows more than just the little concentrated region where the laser beam lands. The light dispersed by the solution also produces a bigger lighted region. (Lars, 2019)

The dispersed light has the greatest intensity at the centre and becomes weaker as it moves away from it. The dispersed light on the screen would not have diminished as quickly as it did with increasing distance from the centre if the solution had been diluted skim milk instead of standard full fat milk. The explanation for this appears to be that the particles responsible for light scattering in the two types of milk have different sizes: Casein micelles (spherical protein structures with a diameter of roughly 300 nm) are the scatterers in skim milk, whereas fat globules (spheres) with a diameter of approximately 3 m, or ten times greater, are the scatterers in ordinary milk. (Lars, 2019)

Figure 2.7. is an illustration of the notion that tiny particles scatter light more uniformly in all directions, but bigger particles prefer forward scattering. This means that the way the intensity of scattered light changes as a function of the angle at which it scatters carries information about the size of the particles that scatter the light. Furthermore, if the particle concentration is known, the molecular weight may be calculated in this manner. A screen is obviously insufficient to make any effective use of light scattering. Instead, a light detector is used to determine the intensity of scattered light at different scattering angles. (Lars, 2019)

2.3 Brief History of Dynamic Light Scattering

Fluctuations in the density of condensed media cause local inhomogeneities, which cause light to be scattered at angles other than the forward direction, as Smoluchowski (1908) and Einstein (1910) discovered at the turn of the century. The spectral profile of the dispersed light, however, was not calculated by these scientists. Brillouin (1914, 1922) demonstrated that variations propagating at v caused "doublets" that were frequency-shifted by an amount proportional to from the incoming light's frequency. Gross (1930,1922) detected this doublet as well as a center peak of unshifted frequency in his experiments. The centre, or Rayleigh, peak was accurately attributed to non-propagating entropy fluctuations by Landau and Placzek (1934). Despite the fact that the spectrum profiles of scattered light carried a lot of information, the inherent linewidth of the incident radiation was too wide to allow meaningful information contained in the very modest frequency changes to be retrieved except in the rarest conditions. With the introduction of the laser in the 1960s, this position was transformed. BSA monomers and dimers were resolved by Ware and Flygare. Doppler shift spectroscopy (DSS) or electrophoretic light scattering is the name of this method (ELS).(Kenneth S, 1990)

In 1971, Ware and Flygare (1971, 1972) published DLS tests on bovine serum albumin (BSA) in the presence of a static electric field, E°. This was the first substantial change in the light scattering technique. E° has the effect of superimposing a constant drift velocity on the random Brownian motion of the charged particles, proportional to the species' electrophoretic mobility. As a result, the resultant spectral density is made up of peaks that are Doppler-shifted from the center.(Kenneth S, 1990)

DLS techniques were first used to determine the molecular weights and shapes of molecules. The development of hydrodynamic theories for complex, irregular-shaped particles coincided with the development of DLS methods, which was no coincidence. Kirkwood and Riseman (1948), Kirkwood (1949,1954), and Zimm (1956) pioneered the beaded string subunit model for polymers, but it took almost two decades for Bloomfield et al. (1967), Rotne and Prager (1969), Yamakawa (1970), Yamakawa and Tanaka (1972), Yamakawa and Yamaki (1972, 1973), McCammon et al. (1975), McCammon and Deutch (1976), Garcia de la (1977)

DLS techniques were widely accepted by the scientific community in the mid-1970s, owing to their efficacy in determining molecular weights and shapes. New knowledge about specific systems began to emerge as more groups began to employ these strategies. Instrumentation advancements resulted in more precise and accurate data. Minor

inconsistencies between theory and experiment were quickly discovered. These differences led to the development of more advanced theories and methods of analysis, as well as novel procedures for sample preparation and handling. (Kenneth S, 1990)

2.4 Dynamic Light Scattering (DLS)

It is known that Brownian motion depends on the velocity of the particles size, these sizes can be estimated by observing the fluctuation corresponding to this velocity. Thus, abstract particles disperse in a solution are in a constant Brownian motion. The particle size and distribution can be obtained, by the autocorrelation function of the observed fluctuation. Dynamic light scattering (DLS) uses principle of Brownian motion and provide size information of a wide range of particles easily and accurately. (Masahiko, 2019)

DLS is widely preferred by many researchers because the size information of particles, molecular aggregates, and emulsion droplet is extremely important. However, data analysis of DLS is based on the assumption that the particles are uniform and spherical. It should also be noted that the obtained size includes a solvated layer around the particles. Due to its nature, other equipment must be used to obtain detailed information such as the shape. The principle and detailed analysis method by DLS measurement will be described in this section.

It has been proven that while suspended in solution, macromolecules are in constant interaction with solvent molecules. These interactions result in random motion of the macromolecule, more commonly known as Brownian motion. Malvern Instruments provides a brief introduction to dynamic light scattering, a technique that uses the natural Brownian motion to determine particle size. To determine particle size by Brownian Motion analysis it is necessary to determine the translational diffusion coefficient (D), which can be characterized as the speed of diffusion or Brownian Motion. The larger the particle, the slower the Brownian motion will be and vice versa. Certain properties of solutions must be known for Dynamic Light Scattering to produce valid results. For example, the temperature of the solution must be accurately known in order to characterize solution viscosity. Temperature must also be held stable or else convection currents in the sample will cause non-random movements that will alter the measurements for the translational diffusion coefficient, ultimately corrupting the correct interpretation of particle size (source, Malvern Instruments Ltd).

Dynamic light scattering (DLS), also known as Quasi Elastic Light Scattering (QELS), is a non-invasive, well-established technique for detecting the size and size distribution of

molecules and particles in the submicron range, and in some cases, as small as 1nm using the newest technology. The characterisation of particles, emulsions, or molecules that have been disseminated or dissolved in a liquid is a common application of dynamic light scattering. Laser light is dispersed at varying intensities due to Brownian motion of particles or molecules in suspension. Using the Stokes-Einstein connection, the velocity of Brownian motion and hence the particle size may be calculated from these intensity variations. (Source, Malvern Instrument)

Dynamic Light Scattering is one of the most often used techniques for determining particle size. When a monochromatic light beam, such as a laser, is shone upon a solution containing spherical particles moving in Brownian motion, the light undergoes a Doppler shift, altering the wavelength of the incoming light. This variation is proportional to the particle's size. By measuring the particle's diffusion coefficient and utilizing the autocorrelation function, it is feasible to compute the sphere size distribution and provide a description of the particle's mobility in the medium. This approach has several advantages: first, the experiment is quick, and it is nearly entirely automated, thus no prior knowledge is necessary for regular measurements. Furthermore, the development expenses for this technology are low. The majority of commercial "particle sizing" devices employ red light and operate at just one angle (90°). (675 nm). The influence on concentration is usually ignored in these systems. The approaches can be significantly extended, as well as more involved and expensive, by using more advanced experimental equipment (projector, short wavelength light source). (Pecora, 1985)

Although dynamic scattering may differentiate whether a protein is a monomer or dimer in theory, it is far less precise than conventional light scattering or sedimentation velocity in distinguishing small oligomers. Dynamic scattering has the benefit of being able to evaluate samples comprising a wide range of species with vastly varied molecular weights (e.g., a native protein and various aggregation sizes) while detecting very little levels of the higher mass species (0.01% in many situations). Furthermore, because there is no chromatographic separation involved, there is no risk of protein aggregates being lost within a chromatographic column (a major concern when employing SEC to characterize aggregates). (Pecora, 1985)

2.4.1 What to expect?

- Measurement of particle sizes ranging from 1 nm to 5 m.
- Light-based noncontact measurement allows for unharmed sample measurement.
- If the viscosity and refractive index of the solvent are known, particle size may be calculated.

2.4.2 Theory of Dynamic Light Scattering

The theory of dynamic light scattering measurement is shown in Figure 2.1, as well as a simplified technique for determining particle size. The particles are continually diffusing in the solution in Brownian motion, as stated in the introductory section. As a result of interference, the light scattering strength varies owing to time-dependent spatial location changes of the particles. The diffusion coefficient is calculated by examining autocorrelation from the temporal variation of the scattering intensity. The Stokes-Einstein equation (Eq. 2.1) may be used to calculate the hydrodynamic radius if the molecules are spherical and uniform. (Masahiko, 2019)

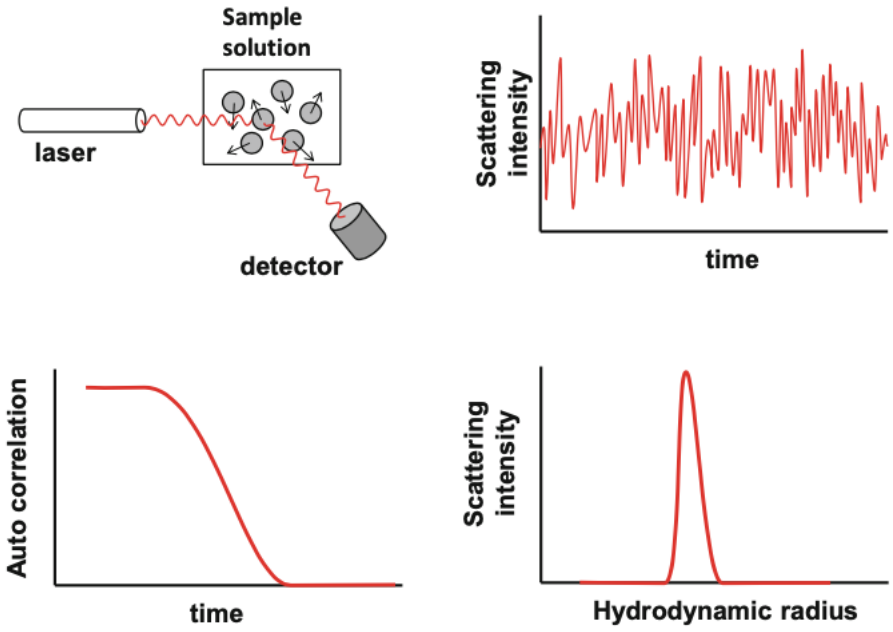

Figure 2.9 steps involved in getting a particle size distribution using dynamic light scattering measurements. (Masahiko, 2019)

$$D = \frac{K_B T}{3\pi\eta d}$$

Equation 2. 3 (Masahiko, 2019)

D: Diffusion coefficient, KB:Boltzmann constant, T: Temperature, η: Viscosity and d: Hydrodynamic diameter. From the particle size information, the formation of molecular aggregate can be confirmed.

2.5 Understanding the Data

2.5.1 Quality of autocorrelation function graph

The derived size distribution graph (right bottom in Figure. 2.8) is commonly used to determine particle size; however, the autocorrelation function graph must be carefully analysed. As a result, it's critical to determine if the autocorrelation function graph is suitable for study. Examples of autocorrelation function graphs are shown in Figure 2.9, and their meaning is as follows:

- The autocorrelation curve in Figure. 2.10a contains two inflection points, showing the presence of two distinct sizes of particles in the sample, with tiny particles experiencing quick attenuation and big particles experiencing slow attenuation. (Masahiko, 2019)

- The autocorrelation curve in Figure 2.10b remains constant for a while before attenuating, however it does not totally fade with time. This graph depicts the effect of scattering by very big particles caused by bubble and dust pollution. After a centrifugation or filtering operation, re-measuring is necessary if such a curve is seen. (Masahiko, 2019)

- In Figure 2.10c, an irregular function can be seen early in the attenuation curve. When the single solvent is devoid of particles, this occurrence is common. As a result, the curve type in Figure 2.10c shows that the particle sizes are too tiny or that the particle concentration is too low. To enhance the scattered light intensity from tiny particles or to increase particle concentration, the laser intensity must be raised. (Masahiko, 2019)

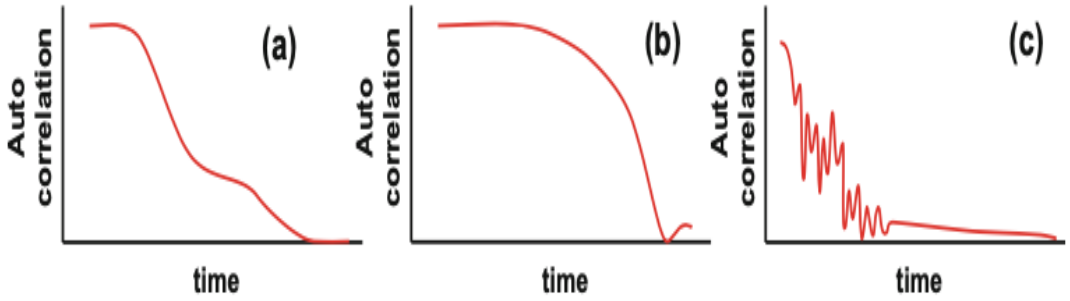

Figure 2.10 Autocorrelation function graph requiring attention (Masahiko, 2019)

2.6 Types of Particle Size Distribution

DLS produces three different size distributions: scatter intensity, volume, and number distribution. The disparity between volume and number distribution is seen in Figure 2.11. The intensity of scattered light is proportional to the particle volume. Because the radius cubed equals the volume, big particles produce great dispersed intensity even in tiny numbers. As a result, it's critical to identify what kind of objective data is needed from DLS measurements, and volume distribution is frequently utilized for molecular aggregation by surfactants, whereas number distribution is employed for bulky monomers and solid microparticles. (Masahiko, 2019)

r	1	5	10	20
r^3	1	125	1000	8000
n	1000	200	100	5
n (%)	76.6	15.3	7.7	0.4
V (%)	0.6	15.1	60.2	24.1

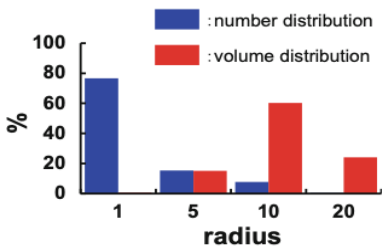

Figure 2.11 Difference between number and volume distribution (Masahiko, 2019)

2.6.1 What to be conscious of

- The assumption that the particles are homogeneous and spherical is used in DLS data processing. Other equipment is necessary to gather precise information such as the shape due to its feature. It's also vital to remember that the size obtained includes a solvated layer around the particles. (Masahiko, 2019)

- Since the Stokes-Einstein equation (Eq. 2.1) is utilized for analysis, the viscosity and refractive index of the solution are needed for correct measurement. (Masahiko, 2019)

- When extraneous substances (dust, bubbles, etc.) enter the measuring sample, their scattering intensity is measured to be higher than the target particle's. As a result, utilizing a filter to avoid contamination of foreign chemicals is critical. (Masahiko, 2019)

- Multiple dispersed lights impact the sample solution when it is overcast at high concentration. As a result, a low sample concentration is preferred. (Masahiko, 2019)

2.7 Particle Size Analysis

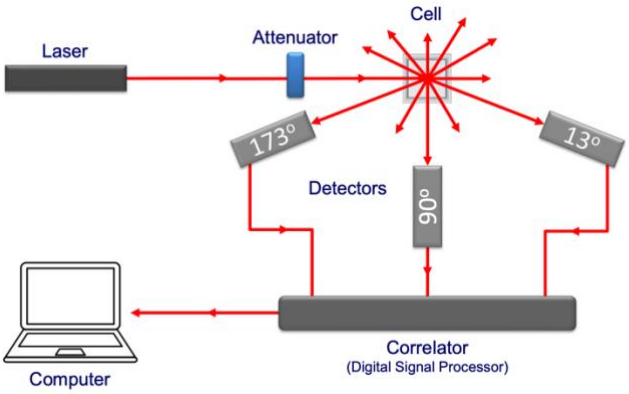

Zetasizer	Detection angle
Ultra	173°, 90°, 13°
Pro	173°, 13°
Nano ZS	173°, 13°
Nano S	173°

Figure 2.12 Optical configuration of zetasizer instrument (Figure source, A.P Instrument)

Zetasizer is an instrument that was used to perform measurement of particle size distribution and zeta potential of the nanodiamond solution. Figure 2.4 shows the optical configuration of the Zetasizer instrument.

As mentioned previously Brownian motion is the random movement of particles caused by the bombardment of surrounding solvent molecules. The velocity of Brownian motion is proportional to the diffusion coefficient (D) as since in Eq. 21. Small particles disperse quickly while larger particles take time to disperse. See Figure 2.12 below:

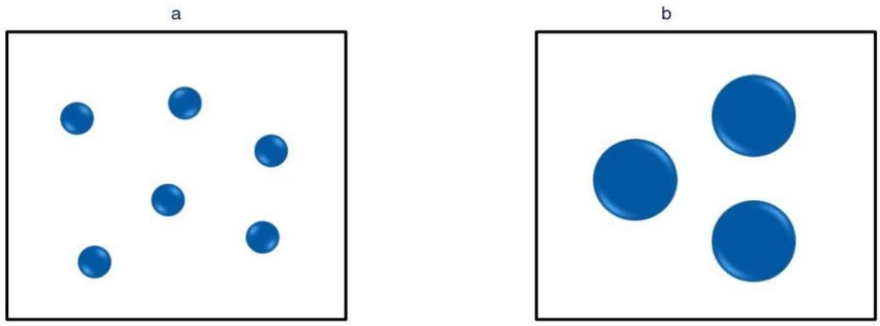

Figure 2.13 shows the two types of particle size, Figure 2.13a shows smaller particle dispersion and Figure 2.13b shows large particle dispersion (Figure source, A.P Instrument)

2.8 Hydrodynamic Diameter

The diameter measured by the DLS method refers to the particle's velocity in the liquid and is referred to as the hydrodynamic diameter. It's calculated as the diameter of a sphere with the same diffusion coefficient as the particle being measured.

Figure 2.14 shows the particle diameter, hydrodynamic diameter and its thickness (Figure source, A.P Instrument)

2.8.1 Hydrodynamic Diameter ionic strength effect

From Figure 2.14 the thickness of the electric double layer is 1/K (Debye length). It is determined by the medium's ionic content. The double layer is thicker when the medium has a low ionic content (e.g., DI water).

2.8.2 Hydrodynamic Diameter surface modification effect

The diffusion will be slowed by the layer of molecules on the particle's surface, which will impact the hydrodynamic diameter. (Figure source, A.P Instrument)

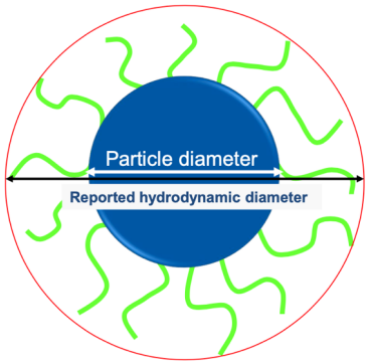

Figure 2.15 shows the surface modification of the hydrodynamic diameter (Figure source, A.P Instrument)

DLS measures the fluctuations in the intensity of light scattered due to the Brownian motion and the velocity of the scattering depends on the size of the particles. The figure below shows an example

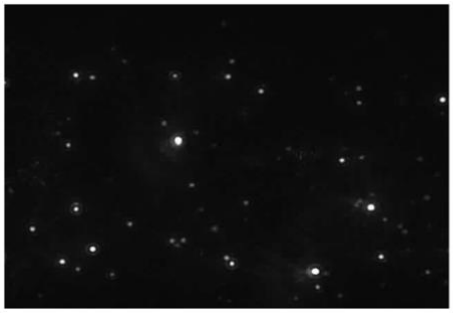

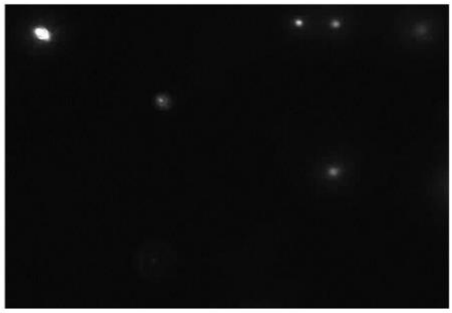

Figure 2.16 shows small and larger particles fluctuation intensity (Figure source, A.P Instrument)

Small particles refer to high diffusion coefficient with rapid intensity changes while large particle refers to low diffusion coefficient with slow intensity fluctuations

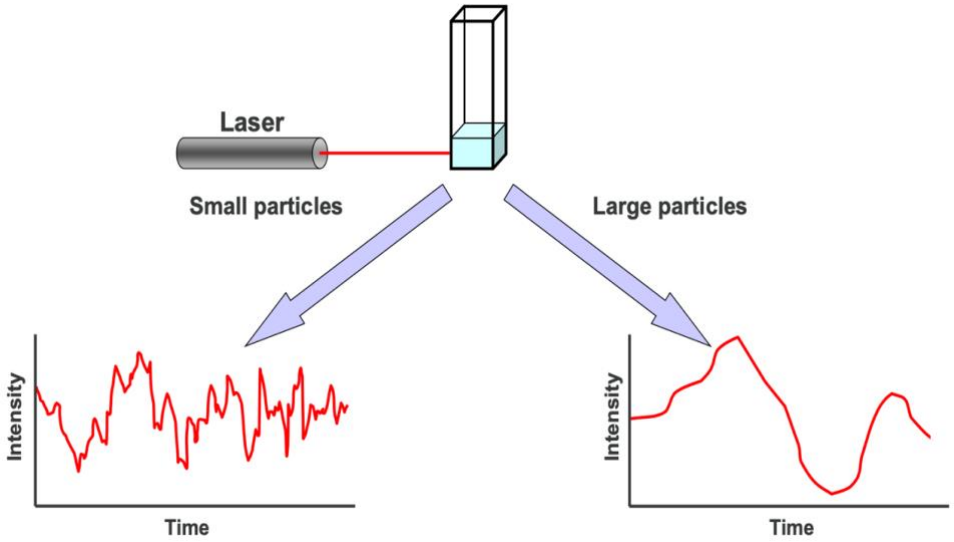

Figure 2.17 shows the particle distribution curve in time. (Figure source, A.P Instrument).

The smaller particles have a greater diffusion coefficient and vary quicker over time than bigger particles.

2.9 Summary of DLS measurements

2.9.1 Correlation

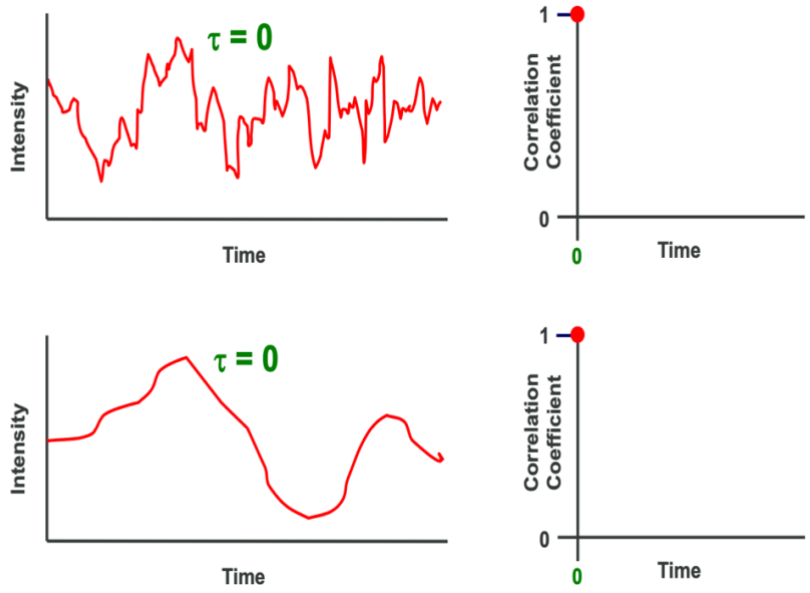

Figure 2.18 shows the particle distribution graph in time = 0 (Figure source, A.P Instrument)

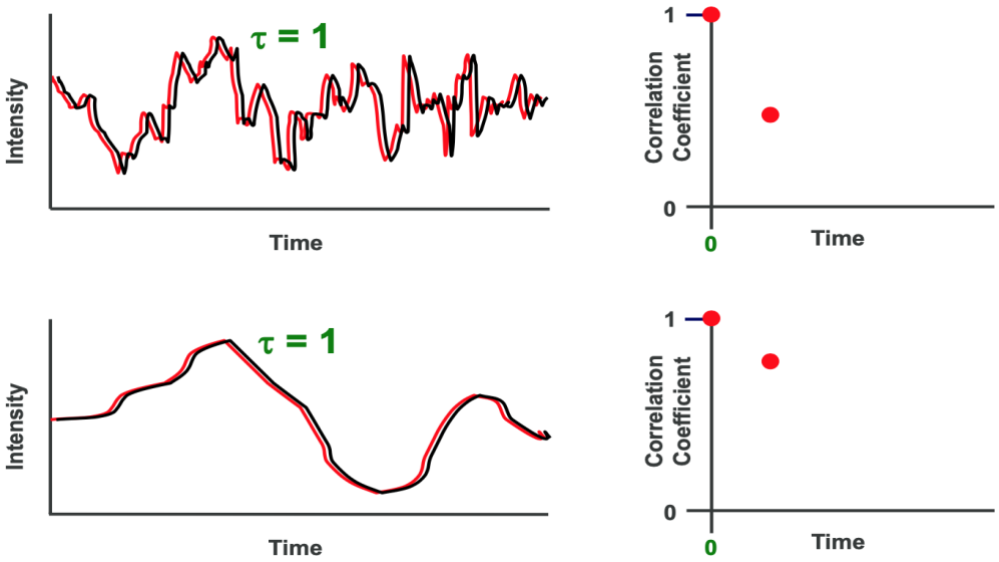

Figure 2.19 shows the particle distribution graph in time = 1 (figure source A.P Instrument)

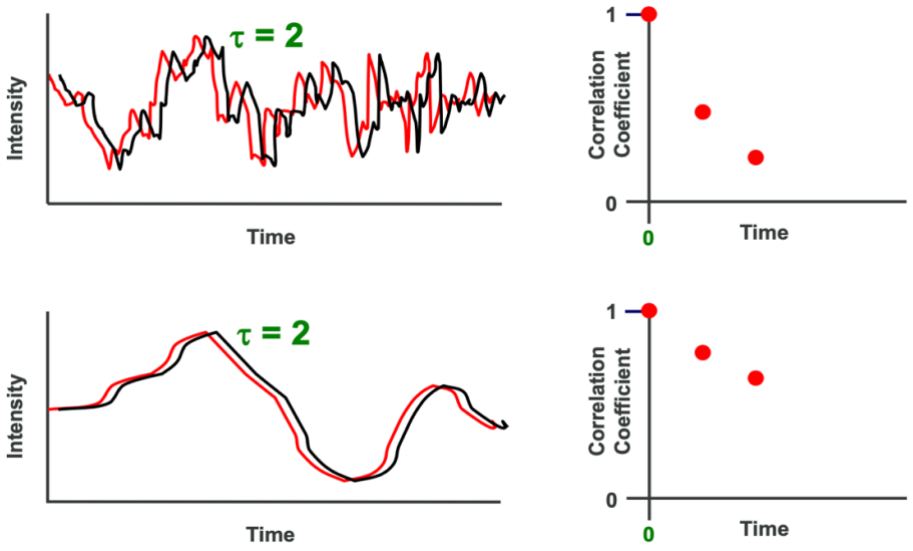

Figure 2.20 shows the particle distribution graph in time = 2 (figure source A.P Instrument)

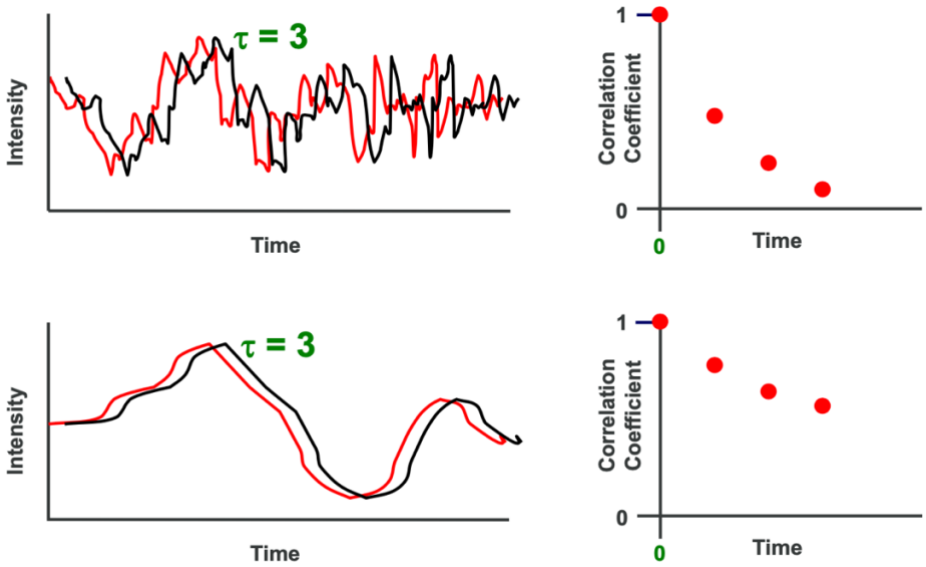

Figure 2.21 shows the particle distribution graph in time = 3 (figure source A.P Instrument)

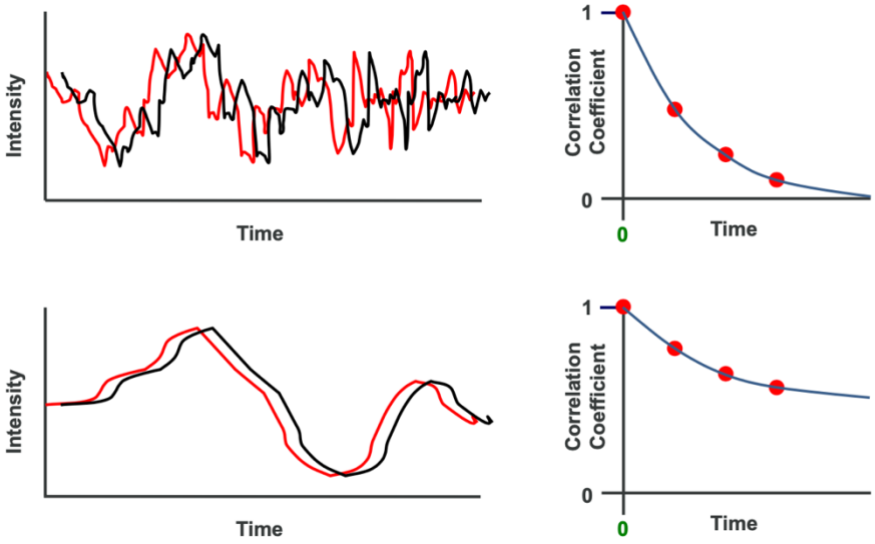

Figure 2.22 shows the correlation of particles at various time away from its origin (Figure source, A.P Instrument)

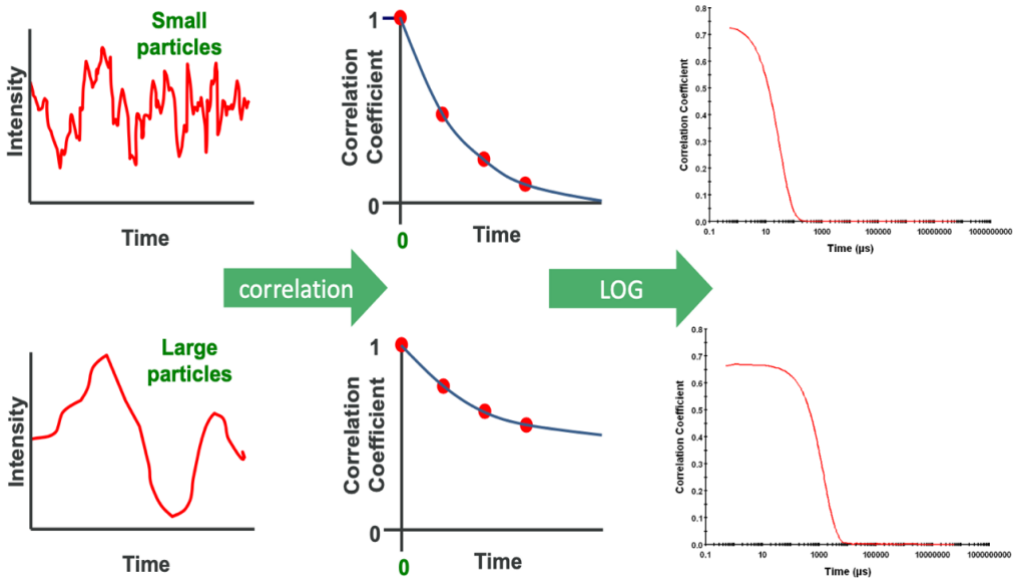

Figure 2.23 shows the correlation of particles at various time (figure source, A.P Instrument)

2.9.2 Correlogram

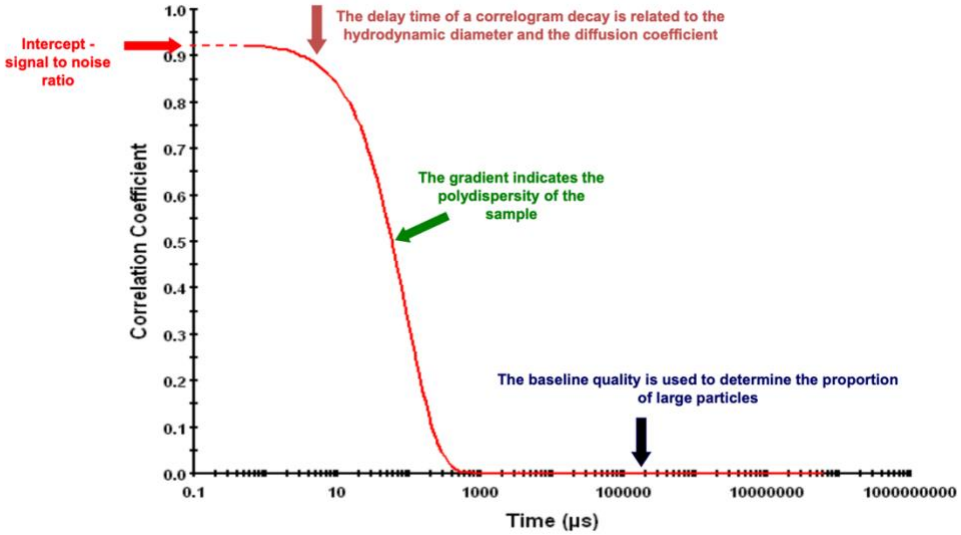

Figure 2.24 The time delay of correlogram degradation (Figure source, A.P Instrument)

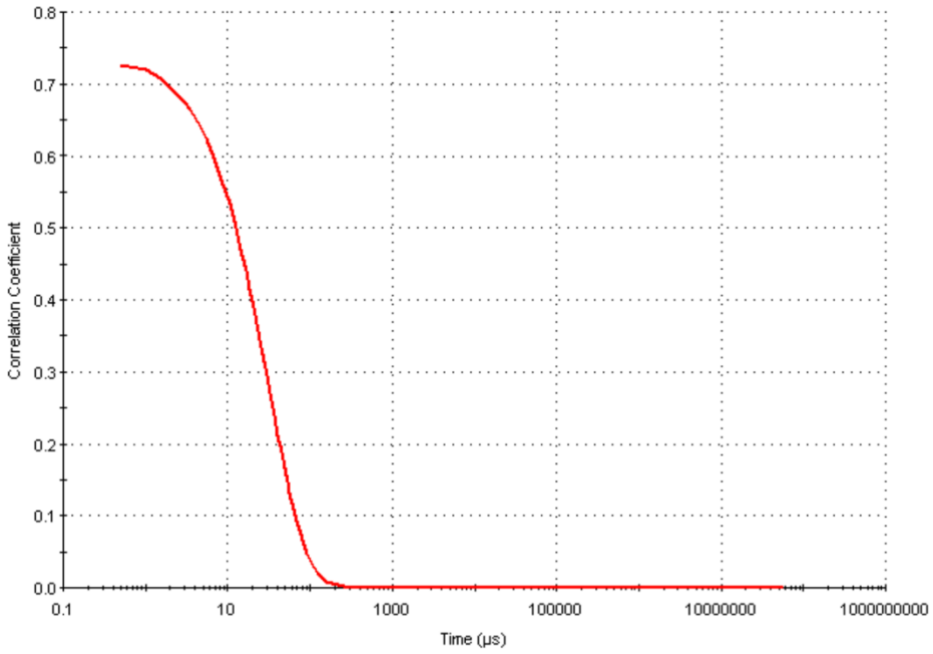

Figure 2.25 show a correlation of small particles (Figure source, A.P Instrument)

2.9.3 Comparison of correlogram

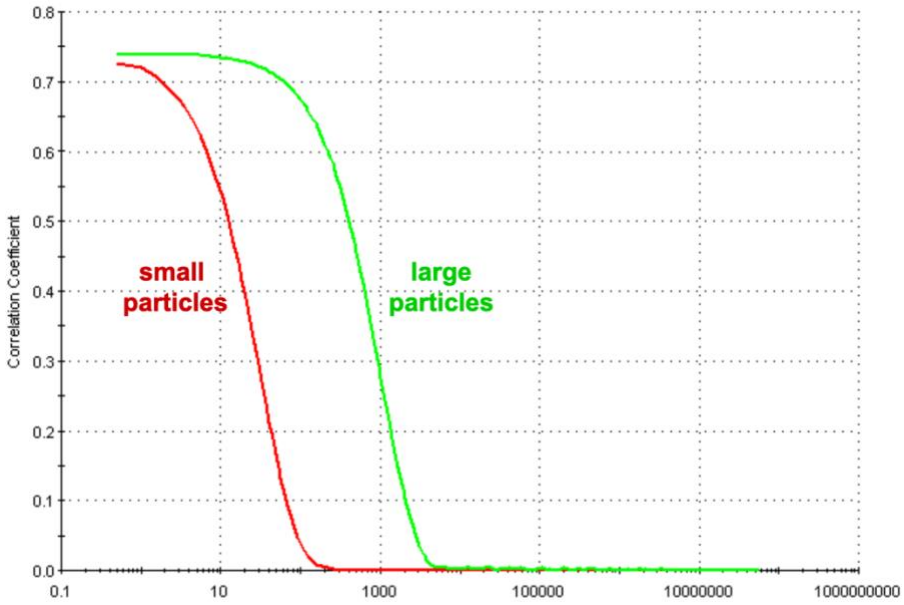

Figure 2.26 Correlation between smaller particles and larger particles (Figure source, A.P Instrument)

Figure 2.18 demonstrates that the particle distribution is in phase with time, whereas Figures 2.19 and Figure 2.20 illustrate that as time advances, the particle distribution tends to drift out of phase. Higher intensity distributions with respect to time indicate smaller particle sizes, and lower intensity distributions with respect to particle size indicate larger particles. Figures 2.21 and 2.22 depict the particles' steady drift from their initial position as the passage of time goes on. The graph demonstrates how the size of the particles affects the intensity of the particle size distribution because smaller particles diffuse more quickly than larger particles do during the same time period.

Depending on their sizes, particles of various sizes will diffuse at varying rates in a particular medium. An overview of the intensity of how particles of different sizes distributed in the same period of time when diffused in the same medium is shown in Figures 2.23 and 2.24. While Figure 2.25 and 2.26 is showing the performance graph of how smaller particles and larger particles were distributed. The curve represents the rate of intensity at which the particles are moving with respect to time when place in the same dispersing medium.

2.9.4 Obtaining data from a correlogram - Nano series

The particle size is determined by studying the correlogram using various techniques.

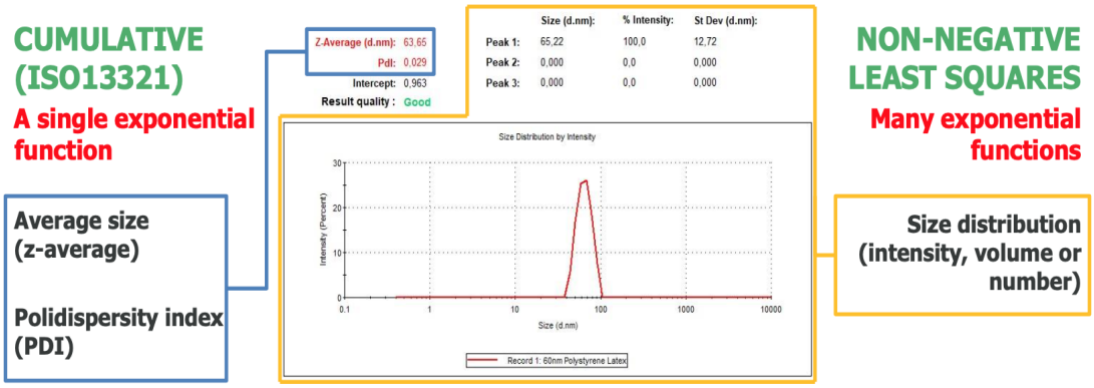

Figure 2.27 shows Nano Series techniques for obtaining data from a correlogram (Figure source, A.P Instrument)

2.9.5 Getting data from a correlogram - pro / ultra-series

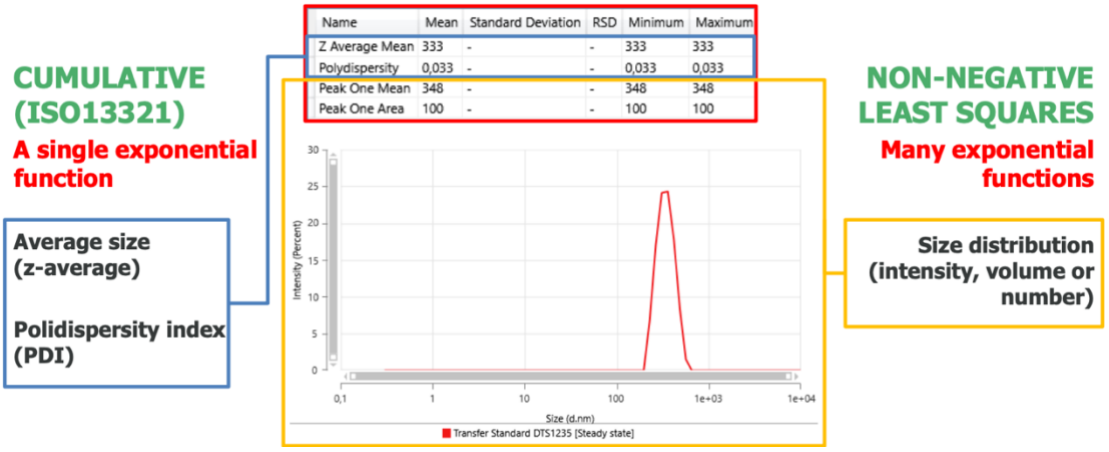

Figure 2.28 shows Pro / Ultra series techniques for obtaining data from a correlogram. (Figure source, A.P Instrument)

Figures 2.27 and 2.28 illustrate, the variety of ways to extract data from a correlogram from a single particle size measurement. It displays information on distribution volume, distribution intensity, average size measurement, and polydispersity. From the figure we can see the quality of the solution prepared from different particle sizes. Smaller particle produces better dispersion when compared to larger particles when placed in the same dispersing medium.

2.10 Obtaining information on particle size

1. The particle size distribution depicted is derived from the Non-Negative Least Squares (NNLS) study.
2. The particle size distribution is a graph illustrating the relative intensity of dispersed light by particles of various sizes.
3. There are 70 size classes, which are organised logarithmically.
4. As with the previous, we obtain an INTENSITY size distribution plot.
5. If the INTENSITY size distribution plot consists of a single smooth peak, there is no need to translate it into a VOLUME size distribution plot using Mie theory.
6. If the INTENSITY size distribution plot has two or more peaks, we may change it to the VOLUME size distribution plot, which will allow us to analyse how significant extra fractions are.
7. The NUMBER size distribution plot is rather unhelpful since a minor inaccuracy in data

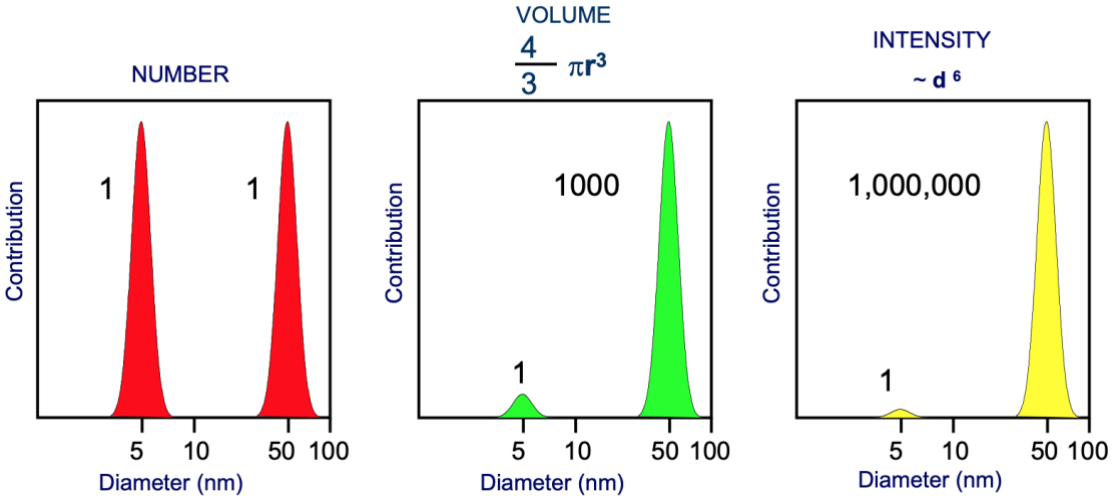

collection might lead to massive inaccuracies in the distribution plot. Figure source, A.P Instrument)2.10.1 Intensity, volume and number distribution plotsFigure 2.29 showing the distribution of Intensity, volume and number distribution. A combination with the same number of 5 and 50 nm particles. (Figure source, A.P Instrument)

2.10.2 Features of Zetasizer - Non-Invasive Back Scattering - (NIBS)

Samples that have been diluted or are made up of little particles

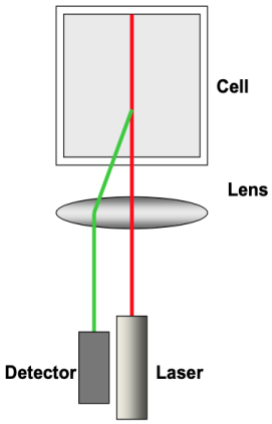

1. Measurement location – half of the cell

2. Increased measurement volume

3. Fewer flares from the cell wall

Based on the smaller sizes of the particles, the volume of particles measure is more and the space required is practically small to perform this operation which will result to more intense and rapid light scattering with longer light path length and reflection.

Figure 2.30 shows Non-invasive back scattering of small particles (Figure source, A.P Instrument)

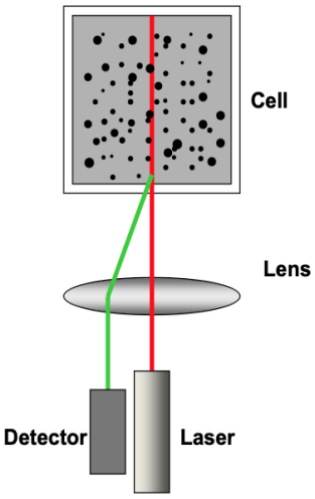

1. Measurement location – behind a wall

2. Shortened light path length

3. Reduced multiple scattering

Due to the larger sizes of the particles, the volume of particles measure is lesser and the space required is practically larger to perform this operation which will result to less intense and slower light scattering with shorter light path length.

Figure 2.31 shows Non-invasive back scattering of large particles. (Figure source, A.P Instrument)

2.10.3 The benefits of employing NIBS are as follows:

- The laser light does not have to travel through the entire sample.
- You may use this to decrease the effect of multiple scattering.
- You will be able to measure more concentrated samples as a result of this.
- Impurities, such as dust particles, scatter light mostly forward.
- As a result, backscatter detection lessens the impact of dust contamination.

2.11 Practical hints for determining a particle size

2.11.1 The DLS technique's top measurement limit

- The DLS approach has an upper limit on the particle sizes that can be assessed.
- The DLS approach is not suited for application when particle movement becomes non-accidental (e.g., in sedimentation).
- The higher range is controlled by the start of the sedimentation process; as a result, it is sample-dependent.
- Suspending particles in a viscous liquid prevents sedimentation, but Brownian motion slows down as a result. (Figure source, A.P Instrument)

2.11.2 The DLS technique's lowest measurement limit

- Concentration of the sample
- Relative refractive index of particles and dispersion Laser power and/or light wavelength
- Sensitivity of the detector
- Optical setup of the instrument

a b

Figure 2.32 zetasizer device for measuring particle size distribution and zeta potential. (Figure source, Malvern instrument)

Chapter 3: Result and Discussion

The analysis is divided into two sessions, which are:

- Set I - Measurement of particle size distribution and Zeta potential, using nanodiamond solution in Zetasizer, by the use of dynamic light scattering techniques.

- Set II - By monitoring and comparing the diverse structural patterns formed by droplets of nanodiamond solution on silicon glass surface, a biological microscope was used to carry out examination of distinct nanodiamond particles.

3.1 Materials and preparation of dispersions

3.1 Set I

3.1.1 Weekly measurements and data

Week one, 10.10mg of ND-2.0 (Detonation Nanodiamond powder) generated by ADAMS nano using the measuring scale was measured. A graduated cylinder was used to measure 10ml of H20 (deionised water) ==> C = 1mg/ml in order to get the right volume of solvent. The ND-2.0 powder was dissolved in H20 to make a solution. After producing the ND-2.0 solution, ultrasonic bath with low power ultrasound was used to homogenise the solution. This bath took 30 minutes to complete. A scheme of the nanodiamond dispersion is shown in figure 3.1.

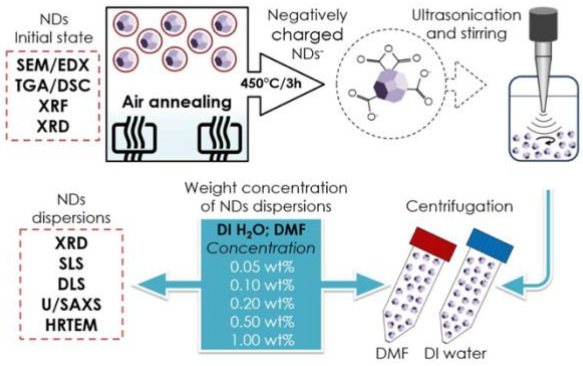

Figure 3.1 showing analytical instruments used and the production method of nanodiamond dispersions. (Tomáš, 2020)

Three particle size distribution measurements were taken, and the summary of the data was also obtained. The findings of the method 1 – Week 1 measurement are shown below in Figure 3.2

Sample Details

Sample Name:	mixture of ND particle with (H20) 1
SOP Name:	mansettings.nano
General Notes:	

File Name:	labDay1 (Nd with deioniz...	**Dispersant Name:**	Water
Record Number:	1	**Dispersant RI:**	1.330
Material RI:	2.42	**Viscosity (cP):**	0.8872
Material Absorbtion:	0.000	**Measurement Date and Time:**	19 October 2021 15:55:13

System

Temperature (°C):	25.0	**Duration Used (s):**	60
Count Rate (kcps):	475.7	**Measurement Position (mm):**	0.85
Cell Description:	Disposable sizing cuvette	**Attenuator:**	5

Results

			Size (d.n...	**% Intensity:**	**St Dev (d.n...**
Z-Average (d.nm):	167.0	**Peak 1:**	199.9	97.6	85.58
PdI:	0.241	**Peak 2:**	4806	2.4	722.0
Intercept:	0.933	**Peak 3:**	0.000	0.0	0.000
Result quality	Good				

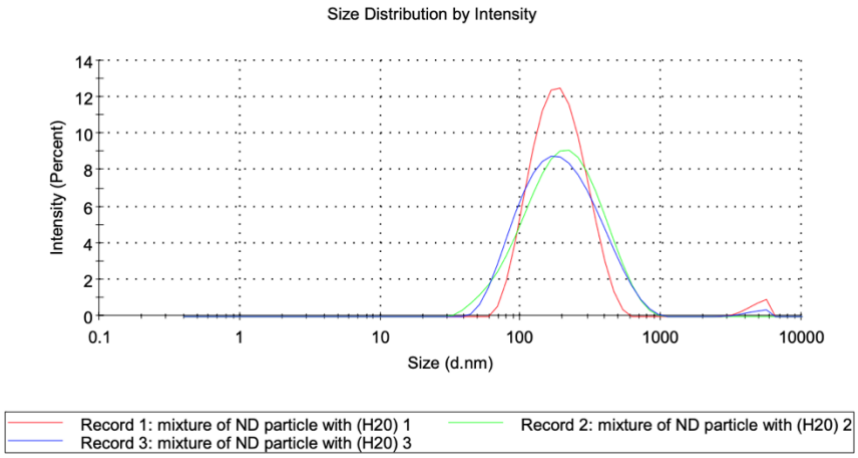

Figure 3.2 graph of average measurement of particle size distribution

Week two, a measuring scale was used to weigh 10.10mg of ND-2.0 (Mono Crystalline Nanodiamond powder) with a size range of MSY 0.25 - 0.75 micron to acquire an accurate number. The amount of powder used was 10.13mg, and the quantity of solvent used was 10ml H20 (deionized water) ==> C = 1mg/ml. Following the creation of the ND-2.0 solution, the solution was homogenised using the ultrasonic bath method (Ultrasonic bath use low power ultrasound). This bath took 30 minutes to complete. For the week two analysis, the configuration and set up were based on Figure 3.1.

Three particle size distribution measurements were taken, and the summary of the data was also obtained. The findings of the method 1 – Week 1 measurement are shown below in Figure 3.3

Sample Details

Sample Name:	Mono_Crystalline_nano_powder_H20_solvent 1
SOP Name:	mansettings.nano
General Notes:	

File Name:	labDay2 (Monocrystallin...	**Dispersant Name:**	Water
Record Number:	1	**Dispersant RI:**	1.330
Material RI:	2.42	**Viscosity (cP):**	0.8872
Material Absorbtion:	0.000	**Measurement Date and Time:**	26 October 2021 15:37:33

System

Temperature (°C):	25.0	**Duration Used (s):**	60
Count Rate (kcps):	431.4	**Measurement Position (mm):**	0.65
Cell Description:	Disposable sizing cuvette	**Attenuator:**	4

Results

			Size (d.n...	% Intensity:	St Dev (d.n...
Z-Average (d.nm):	448.2	**Peak 1:**	489.3	100.0	173.7
PdI:	0.164	**Peak 2:**	0.000	0.0	0.000
Intercept:	0.756	**Peak 3:**	0.000	0.0	0.000
Result quality	Good				

Figure 3.3 average measurement of the particle size distribution and intensity

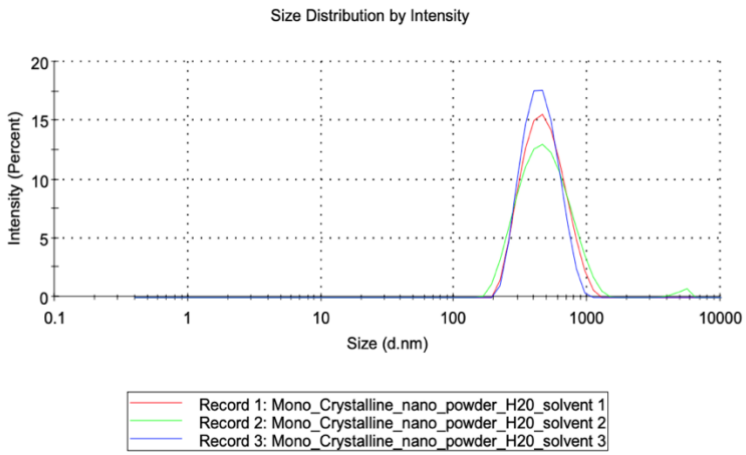

Figure 3.4 average measurement of graph of particle size distribution and intensity

Week three, to get an exact figure, 10.10mg of ND-2.0 (Mono Crystalline nanodiamond powder) with a size range of MSY 0.25 - 0.75 micron and a total of 0.789g of powder was measured. To crush/break down the powder into tiny pieces, WC (tungsten carbide) was used. The solvent used was 10ml H20 (deionized water) ==> C = 1mg/ml. The grinding ball was then put in the grinding jar. The grinding ball has a capacity of 12ml and 45ml. The grinding ball was configured at an RPM (Rotation Per Minute) of 700 at a duration of 7 minutes. The combined weight of the ball and powder was less than 70g. The grinding ball used had a diameter of 3mm, a mass of 48.298g, and a mass of 0.789g of powder.

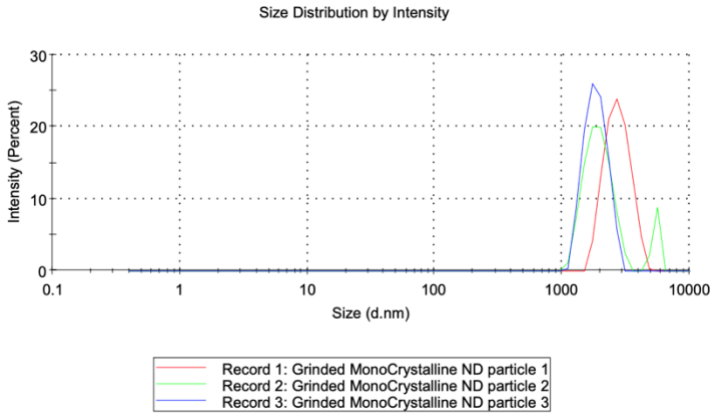

Figure 3. 5 average measurement of graph of particle size distribution

Sample Details

Sample Name:	Grinded MonoCrystalline ND particle 1
SOP Name:	mansettings.nano
General Notes:	

File Name:	labDay3 (Grinded _with_...	**Dispersant Name:**	Water
Record Number:	1	**Dispersant RI:**	1.330
Material RI:	2.42	**Viscosity (cP):**	0.8872
Material Absorbtion:	0.000	**Measurement Date and Time:**	09 November 2021 15:29:43

System

Temperature (°C):	24.9	**Duration Used (s):**	80
Count Rate (kcps):	125.6	**Measurement Position (mm):**	1.05
Cell Description:	Disposable sizing cuvette	**Attenuator:**	3

Results

			Size (d.n...	**% Intensity:**	**St Dev (d.n...**
Z-Average (d.nm):	2976	**Peak 1:**	2740	100.0	614.9
PdI:	0.227	**Peak 2:**	0.000	0.0	0.000
Intercept:	0.775	**Peak 3:**	0.000	0.0	0.000
Result quality	**Refer to quality report**				

Figure 3.6 average measurement of particle size distribution and intensity

Week four, to get an exact number, 10.14mg of ND -2.0 (Mono Crystalline Nanodiamond powder) was weighed for veil 1 and 10.16mg for veil 2, using a measuring scale with a size range of MSY 0.25 - 0.75 micron. For the solvent, 10ml Ethyl alcohol (Ethanol) and Dimethyl Sulfoxide as my alcohol (DMSO). Following the development of the ND-2.0 solution, the ultrasonic bath procedure was used to homogenise it (Ultrasonic bath use low power ultrasound). It took 30 minutes to complete this bath. In the end, an indication showing a lower zeta potential of alcohol solution was observed.

Sample Details

Sample Name:	Ethanol Solution of ND particles 1
SOP Name:	mansettings.nano
General Notes:	

File Name:	labDay_4_Ethanol (Ultra...	**Dispersant Name:**	Ethanol
Record Number:	1	**Dispersant RI:**	1.361
Material RI:	2.42	**Viscosity (cP):**	1.0740
Material Absorbtion:	0.000	**Measurement Date and Time:**	23 November 2021 15:34:16

System

Temperature (°C):	25.0	**Duration Used (s):**	90
Count Rate (kcps):	118.0	**Measurement Position (mm):**	0.85
Cell Description:	Disposable sizing cuvette	**Attenuator:**	3

Results

			Size (d.n...	% Intensity:	St Dev (d.n...
Z-Average (d.nm):	190.9	**Peak 1:**	212.3	100.0	70.43
PdI:	0.095	**Peak 2:**	0.000	0.0	0.000
Intercept:	0.959	**Peak 3:**	0.000	0.0	0.000
Result quality	Good				

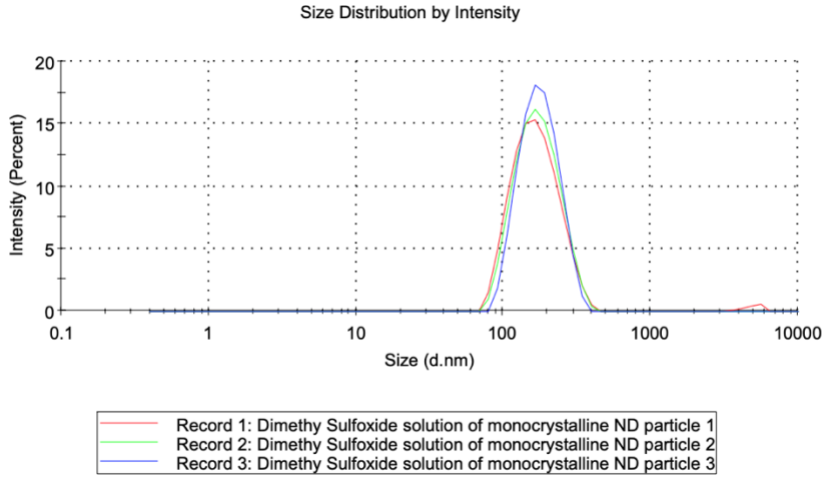

Figure 3.7 Shows the average, measurement of graph of particle size distribution and intensity

Sample Details

Sample Name:	Dimethy Sulfoxide solution of monocrystalline ND particle 1		
SOP Name:	mansettings.nano		
General Notes:			
File Name:	LabDay 4B_ Dimethy Su...	**Dispersant Name:**	Dimethyl Sulfoxide (DMSO)
Record Number:	1	**Dispersant RI:**	1.477
Material RI:	2.42	**Viscosity (cP):**	1.9870
Material Absorbtion:	0.000	**Measurement Date and Time:**	23 November 2021 16:20:04

System

Temperature (°C):	25.0	**Duration Used (s):**	60
Count Rate (kcps):	501.8	**Measurement Position (mm):**	0.85
Cell Description:	Disposable sizing cuvette	**Attenuator:**	4

Results

			Size (d.n...	% Intensity:	St Dev (d.n...
Z-Average (d.nm):	158.9	**Peak 1:**	173.1	98.6	61.37
PdI:	0.147	**Peak 2:**	4887	1.4	676.9
Intercept:	0.919	**Peak 3:**	0.000	0.0	0.000
Result quality	Good				

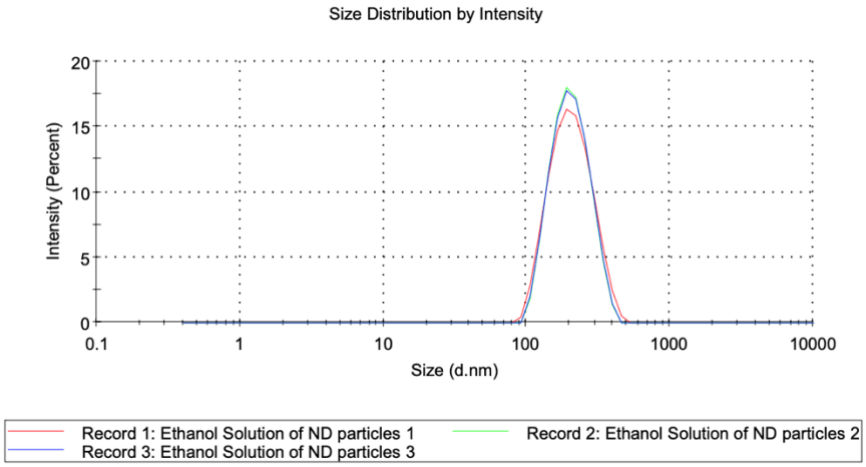

Figure 3.8 Shows the average, measurement of graph of particle size distribution and intensity.

Particle sizes and zeta potentials of the samples were assessed at the conclusion of each measurement. According to the types of modification procedures utilized, the findings from Figures 3.1, 3.2, 3.3, 3.4, 3.5, 3.6, 3.7 and 3.8 demonstrate the quality of these samples. We can see that week 3 exhibits a different result quality based on the kind of strategies utilized to make the solution homogenous. According to the graph in Figure 3.3, the sample contains some noise of a higher volume, which undoubtedly impacted the measurement's quality (particle size measurement and zeta potential) thereby making the test result poor.

3.2 Set II

Diagnosis of structural patterns formed by droplet of nanodiamond particles on silicon glass surface using a biological microscope.Suspensions used were DND, hydrogenated (adamas 5nm) (H-DND) and DND oxidized (adamas 5nm) (O-DND)

3.2.1 Measurement

- SEM map 10x10 (determine the magnification and then assemble the drawing)
- optical microscope - imaging (map surfaces High-resolution)
- DLS of O-DND and H-DND powders in IPA

3.2.2 List of samples

- H -Si (100) + H-DND
- H -Si (100) + O-DND
- Si (100) + O-DND

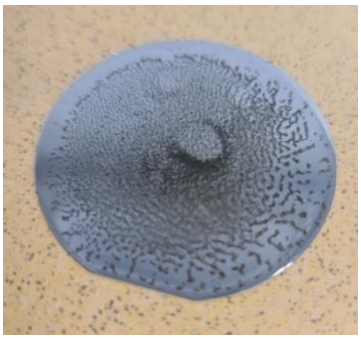

Figure 3.9 showing sample of nanodiamond droplet on silicon glass surface

Using the Orientation of P (111) shown in Figure 3.10, I observed the patterns formed on a silicon glass surface with a biological microscope, then stitched the most interesting region of the patterns together to form a structure, and observed how the different suspensions form different patterns on the silicon surface. These structures were all unique, and their formulation was determined by the solution.

3.2.3 Silicon Substrate

- (111) oxidized (O-(111))
- (111) hydrogenated (H-(111))
- (100) oxidized (O-(100))
- (100) hydrogenated (H-(100))

The surface pattern and configuration angle of the silicon substrate represented by (111) oxidized (O-(111)) lacks hydrogen from its makeup. Its structure is entirely made up of oxygen molecules. The surface structure and configuration angle of a silicon substrate made up mostly of hydrogen molecules are represented as (111) hydrogenated (H-(111)). Having only one sort of element in its molecular structure could make a solution of this type configuration unstable. The angle of this substrate is shown in Figure 3.10 below. While the silicon substrate (100) oxidized (O-(100)) represents the structure configuration of oxidize or hydrogenated substrate which may likely have equal amount of oxygen and hydrogen present in its molecular formation. Structures like this with molecular angle (100) may be practically more stable than structures with (111) configuration. The results of the analysis are found in Figure 3.12, 3.13 and 3.14 respectively. And for this analysis to have a precise result, a consistent configuration of a particular angle should be utilized.

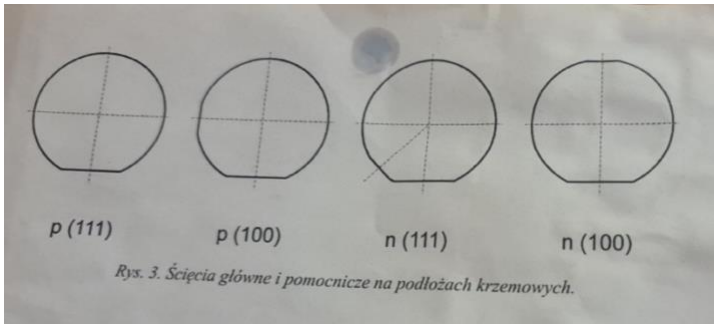

Figure 3.10 configuration for measurement of the droplet on silicon glass surface

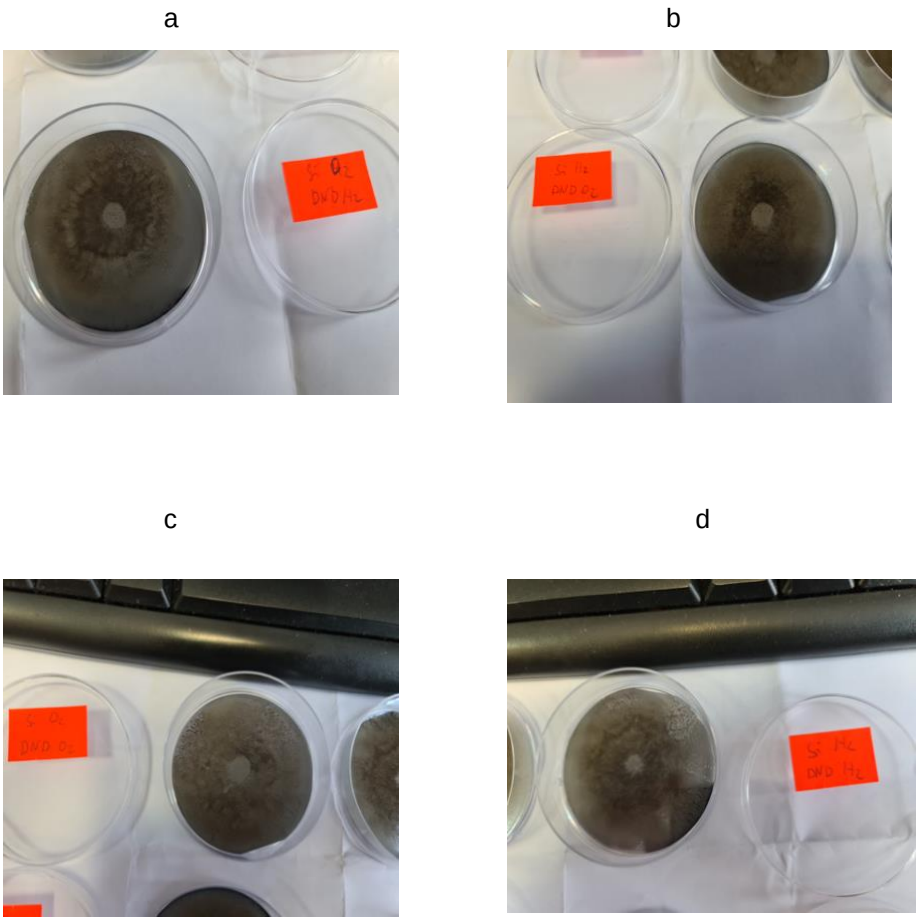

Figure 3.11 showing prepared sample of ND solution droplet and silicon glass

The top view of each sample utilized for set II analysis is displayed in Figure 3.11. A silicon glass containing nanodiamond solution droplets is within the cylindrical containers. These various silicon glass surfaces correspond to the silicon substrate samples that were displayed in chapter 3.2.3 above. A biological microscope can be used to view the structural patterns that these solutions create on the silicon glass surface. Figures 3.12, 3.13, and 3.14 below display the outcomes.

3.2.4. Analysis using hydrogenated denotation nanodiamond solution on silicon glass (Si H DND)

Calibration
Length= 1000
TotalPixel =2167.325
Unit=\x3bcm
UnitPixel= 0.046139826744950575
Resolution= 3072x3063

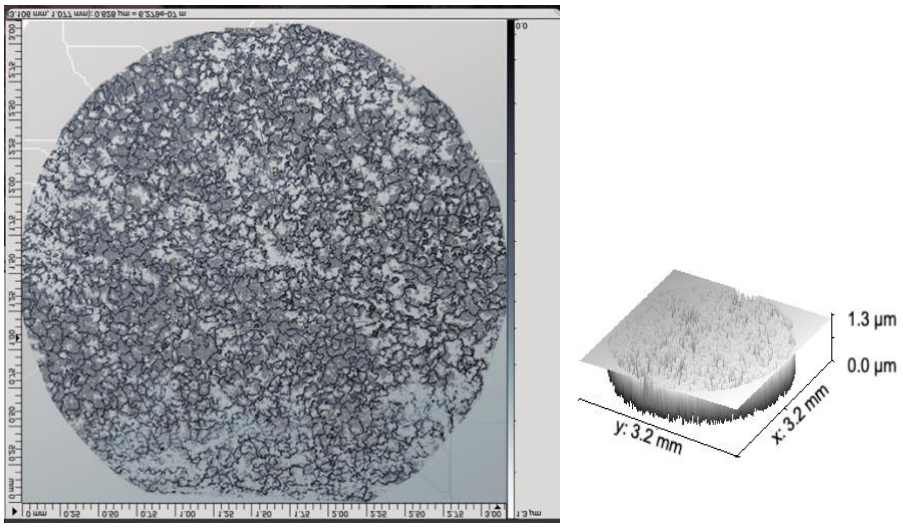

Figure 3.12 showing structure of Si H DND sample. The white patterns are the Hills (High) while the dark patterns are valleys(low)

Table 3.1 showing the analytical data of Figure 3.12 structural analysis

Δx [µm]	Δy [µm]	φ [deg]	R [µm]	Δz [nm]
-622.45175	-353.76754	150.388468	715.95926	-444.97183
205.991228	-707.53509	73.7676493	736.911315	2.49121202
913.526316	58.2149123	-3.6462712	915.379323	-26.30093
-22.390351	-850.83333	91.5074358	851.127892	-522.20691
156.732456	-640.36404	76.2469294	659.265622	-49.614176
-1061.3026	-197.03509	169.482554	1079.43786	-18.414557

Dimension: Total size of silicon glass surface is about 70000 ~ 73000µm and the size measured is about 45000 ~ 48000µm. Discussion of table 3.1 is on chapter 3.3.2

3.2.5 Analysis using hydrogenated and oxidized denotation nanodiamond solution on silicon glass (Si H2 DND O2)

Calibration
Length= 1000
TotalPixel =2167.325
Unit=\x3bcm
UnitPixel= 0.046139826744950575
Resolution= 3072x3063

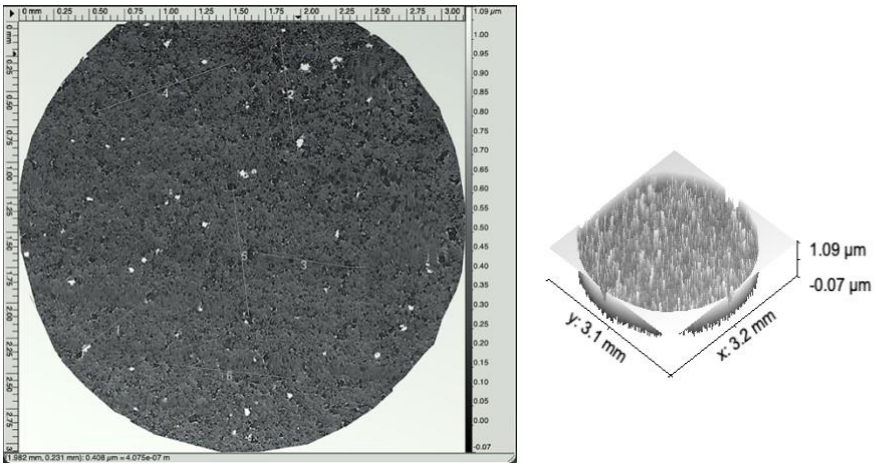

Figure 3.13 structure of Si H2 DND O2 sample. The white patterns are the Hills (High) while the dark patterns are valleys(low)

Table 3.2 showing the analytical data of Figure 3.13 structural analysis

Δx [µm]	Δy [µm]	φ [deg]	R [µm]	Δz [nm]
528.41228070	-411.9824561	37.94215335	670.03662778	6.73481935
102.99561404	752.31578947	-82.20439798	759.33335473	33.47970372
720.96929825	111.95175439	-8.82637095	729.60943273	374.35648305
962.78508772	-349.2894736	19.94030057	1024.18663414	198.98224419
-116.4298245	-922.4824561	97.19347006	929.80093888	- 36.03017267
1007.56578947	111.95175439	6.34019175	1013.76625286	-29.86367318

Dimension: Total size of silicon glass surface is about 70000 ~ 73000µm and the size measured is about 45000 ~ 48000µm. Discussion of table 3.1 is on chapter 3.3.2

3.2.6 Analysis using oxidized denotation nanodiamond solution on silicon glass (Si O2 DHD O2)

Calibration
Length= 1000
TotalPixel =2167.325
Unit=\x3bcm
UnitPixel= 0.046139826744950575
Resolution= 3072x3063

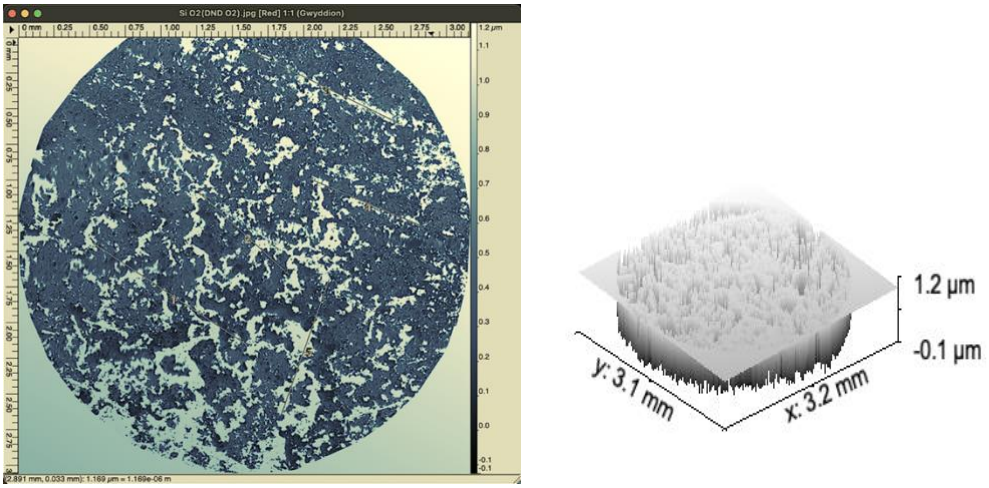

Figure 3.14 showing structure of Si O2 DND O2 sample. The white patterns are the Hills (High) while the dark patterns are valleys(low)

Table 3. 3 showing the analytical data of Figure 3.14 structural analysis

Δx [µm]	Δy [µm]	φ [deg]	R [µm]	Δz [nm]
-1080.6360205	-714.4700962	46.52903573	1295.46969375	105.88235294
-629.62677233	-576.0415151	137.54480438	853.37781759	658.82352941
1089.56689679	535.85257219	-26.18811070	1214.20509046	643.13725490
962.78508772	-349.2894736	19.94030057	1024.18663414	198.98224419
-772.52079158	-325.9769814	157.12194197	838.48039085	-313.7254902
-334.90785762	946.67287754	109.48243426	1004.16772014	-266.6666666

Dimension: Total size of silicon glass surface is about 70000 ~ 73000µm and the size measured is about 45000 ~ 48000µm. Discussion of table 3.1 is on chapter 3.3.2

3.3 Discussion

3.3.1 Set I – using zetasizer

The summary of the numerous results from figures 3.0.2, 3.0.3, 3.0.4, 3.0.5, and 3.0.6 revealed that ND particles act differently depending on the solvent. As a result, each solution has its own set of qualifications.

From my various weeks of experiment, I can give a clear analysis for the performance of the different nanodiamond solution I used. Clearly, I discovered that the techniques I used in making my solution homogenous determines the quality of the solution performance.

From the particle size distribution measurement and the zeta potential measurement, I discovered that the all the solutions with good quality from graph have one similarity in common, they were all made homogeneous by the use of ultrasonic bath with low power ultra sound. Irrespective of the solvent I used, either alcohol or deionised water, so far I made the solution homogenous using ultra sonic bath with low power ultrasound, the quality of the particle size distribution measurement and the zeta potential always comes out good.

I made a variation by using the same nanodiamond particles, the same solvent, but different technique for homogenizing the sample. High energy ball mill i.e. WC (tungsten carbide) to split the powder into tiny fragment and placed the fragment into a griding jar. The grinding ball was configured at an RPM (Rotation Per Minute) of 700 and a duration of 7 minutes, in order to grind the powder and make the solution homogenous. But after using the zetasizer to carry out particle size measure and zeta potential measurement, the quality of the sample turns out poor.

I considered other factors that might have a negative influence on the quality of the solution such as higher concentration of the nanodiamond power than the solvent, but throughout the whole process a consistent measurement range was utilised by using the measuring cylinder to a have precision.

Thus, from the result of my analysis, I observed that to have a better homogenous solution of nanadiamond, ultrasonic bath with low power ultra sound techniques should be utilised, as it can enhance measurement quality of particle size distribution measurement.

3.3.2 Set II – using biological microscope

I discovered that the amount of oxygen and hydrogen in the DND samples influences the type of patterns created on the silicon surface. Observing the structures of the three (3) samples I used (Si H DND), (H2 DND O2), and Si O2 DHD O2), I discovered that the sample with the least amount of structural pattern formation had the same quantity of hydrogen (H) and oxygen (O). For example, in Figure 3.5, we can clearly see on the structural creation of the highs and lows has less patterns when compared to that of Figure 3.4, where sample was primarily composed of hydrogen.

Figure 3.6 depicts a more intriguing pattern formation with a continuous drawing of the highs and lows. Examining the sample, which is entirely composed of oxygen molecules. I noticed that the concentration of hydrogen and oxygen in the sample influences the depth and quality of structural pattern creation on the silicon glass surface.

Tables 3.1, 3.2, and 3.3 shows the data from the structural analysis of Figures 3.10, 3.11, and 3.12. The dimensional difference between the distance between the highs and lows of the nanoparticle droplets on the silicon glass surface is represented by the various values in column Δx [μm], Δy [μm], φ [deg], R [μm] and R [μm]]. These distances are based on the location that was designated as low and high on the silicon glass surface prior to gwyddion's analysis of the structures. It analyzed this structure essentially in a 3D model that showed the values for the patterns' distances from one another and the low patterns that were etched onto the silicon glass surface.

Chapter 4: Conclusion

However, ND particles possess a highly reactive surface surrounding their diamond core, containing a wide variety of chemical functional groups. In the case of detonation ND, the surface of nanoparticles may contain oxygen-containing groups such as carboxylic acids, esters, lactones and amines. In addition, the surface of nanodiamonds (NDs) is partially covered by thin layers of graphitic or graphene-like structures (Krueger 2008).

It has been proven that the surface of NDs can be homogenized using oxidative (oxidizing acids, thermal oxidation) or reductive (hydrogenation, hydrogen plasma treatment, borane reduction). But for my thesis I made used of Ultrasonic bathe with low power ultrasound and the use of High energy ball mill to make my solution homogenous.

According to other researchers' there are a variety of other chemical reactions for functionalizing ND surfaces, mostly with an intent of covalent/non-covalent immobilization and subsequent grafting of complex moieties or larger (bio)molecules. (Liu, 2004)

An example of this method is salinization technique using (3-aminopropyl) trimethoxysilane (APS) application to obtain the covalent attachment of amino acids to the diamond surface. This modification allows efficient grafting of larger bioactive macrostructures such as enzymes or proteins (Krueger 2008).

Further, Bead Assisted Sonic Disintegration (BASD) was found to be an efficient technique to achieve primary particles of NDs in diverse protic/aprotic solvents, including water. Dispersibility of the ND particles in highly polar alcohols and polar or hydrocarbon solvents exemplified the viability of these nanosuspensions with particle size ranging from 4 to 100 nm (Ozawa, 2007).

I used in-house generated deionized water (DI) with a resistivity of 14.3 M.cm at 25°C and Dimethyl Sulfoxide as my dispersing medium (DMSO).

To achieve the requisite dispersion of ND-, the surface of the NDs was changed using an ultrasonic homogenizer. Using a titanium alloy ultrasonic probe with a frequency of operation of 20KHz and an energy conversion of 400kJ into each sample.

The process was then repeated for 40 minutes with continuous stirring to produce grey-colored nano dispersions. The solutions were then centrifuged three times at 700 rpm (70 g) for seven minutes, and the pellets were discarded. My dispersion was subjected to particle size examination utilising dynamic light techniques, as well as diagnostic of structural patterns created on silicon glass when seen under a biological microscope.

Using dynamic light scattering I could measure the particle size distribution of nanodiamond. The optical depth of the samples was lowered utilising backscattering geometry with a scattering angle of 175° to avoid multiple scattering in the DLS tests. Although samples with lower ND concentrations (less than 0.5 wt percent) can be assessed in both forward and reverse scattering geometry to maintain the same experimental setup.

Thus, because the primary purpose of this work was to investigate the impact of particle sizes on dispersion when evaluated in a medium using dynamic light scattering techniques. And also, to diagnose the structural patterns formed by droplets of ND solution on the surface of silicon glass. Thus, the particle size measurement and zeta potential results revealed that both the dispersing medium (water/DMF) and the ND concentration in the investigated range (0.05 – 1 wt percent) had no significance or systematic influence on the size and inner structure of ND aggregates, and thus on the kinetics of ND aggregate formation, but the method of disaggregation is critical. This is based on the two (2) disaggregation methods I employed, which were:

- Centrifugation (Ultrasonic homogeniser) and
- Sonication (High energy ball mill)

Finally, I discovered that the centrifugation method outperforms the sonication method. This is because centrifugation generates a more homogeneous solution than sonication. When assessed in a medium using the DLS technique. While the concentration level of hydrogen and oxygen molecules in the ND samples influences the structural patterns formation. The sample containing only hydrogen generated more patter, the sample containing only oxygen generated more pattern, but the sample with equal level of hydrogen and oxygen concentration resulted to lesser pattern formation.

References

Ballhaus, C., Ryan, C.G., Mernagh, T.P. and Green, D.H., 1994. The partitioning of Fe, Ni, Cu, Pt, and Au between sulfide, metal, and fluid phases: A pilot study. Geochimica et Cosmochimica Acta, 58(2), pp.811-826.

Balasubramanian, G., Chan, I.Y., Kolesov, R., Al-Hmoud, M., Tisler, J., Shin, C., Kim, C., Wojcik, A., Hemmer, P.R., Krueger, A. and Hanke, T., 2008. Nanoscale imaging magnetometry with diamond spins under ambient conditions. Nature, 455(7213), pp.648-651.

Butler, J.E. and Windischmann, H., 1998. Developments in CVD-diamond synthesis during the past decade. MRS Bulletin, 23(9), pp.22-27.

Carlisle, D.B. and Braman, D.R., 1991. Nanometre-size diamonds in the Cretaceous/Tertiary boundary clay of Alberta. Nature, 352(6337), pp.708-709.

Capdevila, R., Arndt, N., Letendre, J. and Sauvage, J.F., 1999. Diamonds in volcaniclastic komatiite from French Guiana. Nature, 399(6735), pp.456-458.

EUGenMed, Cardiovascular Clinical Study Group, Regitz-Zagrosek, V., Oertelt-Prigione, S., Prescott, E., Franconi, F., Gerdts, E., Foryst-Ludwig, A., Maas, A.H., Kautzky-Willer, A. and Knappe-Wegner, D., 2016. Gender in cardiovascular diseases: impact on clinical manifestations, management, and outcomes. European heart journal, 37(1), pp.24-34.

George E., H. and Rondi M., D. 2005 'Diamonds Article', March.
Hammouda, Tahar, and Shantanu Keshav. "Melting in the mantle in the presence of carbon: Review of experiments and discussion on the origin of carbonatites." Chemical Geology 418 (2015): 171-188.

Heaney, P.J., Vicenzi, E.P. and De, S., 2005. Strange diamonds: the mysterious origins of carbonado and framesite. *Elements*, *1*(2), pp.85-89.

Kaur, R. and Badea, I., 2013. Nanodiamonds as novel nanomaterials for biomedical applications: drug delivery and imaging systems. International journal of nanomedicine, 8, p.203.

Kenneth S, S. 1990 An Introduction to Dynamic Light Scattering by Macromolecules. Harcourt Brace Jovanovich, Publishers.

Kovářík, T., Bělský, P., Rieger, D., Ilavsky, J., Jandová, V., Maas, M., Šutta, P., Pola, M. and Medlín, R., 2020. Particle size analysis and characterization of nanodiamond dispersions in water and dimethylformamide by various scattering and diffraction methods. Journal of Nanoparticle Research, 22(2), pp.1-17.

Lars, Ø. 2019 'Light Scattering a brief introduction', University of Copenhagen [Preprint].
Masahiko, A. (ed.) 2019 Measurement Techniques and Practices of Colloid and Interface Phenomena. Springer.

Meen, J.K., Eggler, D.H. and Ayers, J.C., 1989. Experimental evidence for very low solubility of rare-earth elements in C02-rich fluids at mantle conditions. Nature, 340(6231), pp.301-303.

Meyer, H. O. A., and F. R. Boyd. "Composition and origin of crystalline inclusions in natural diamonds." Geochimica et Cosmochimica Acta 36.11 1972: 1255-1273.

Mineralogical Association of Canada Short Course 44, February 2014, Tucson AZ, p. 1-28.

Morse, J.M., Barrett, M., Mayan, M., Olson, K. and Spiers, J., 2002. Verification strategies for establishing reliability and validity in qualitative research. International journal of qualitative methods, 1(2), pp.13-22.

Mochalin, V.N., Shenderova, O., Ho, D. and Gogotsi, Y., 2012. The properties and applications of nanodiamonds. Nature nanotechnology, 7(1), pp.11-23.

Neupane, M., Alidoust, N., Xu, S., Kondo, T., Ishida, Y., Kim, D.J., Liu, C., Belopolski, I., Jo, Y.J., Chang, T.R. and Jeng, H.T., 2013. Surface electronic structure of the topological Kondo-insulator candidate correlated electron system SmB6. Nature communications, 4(1), pp.1-7.

Pecora, R. 1985 Dynamic Light Scattering Applications of Photon Correlation Spectroscopy.

Piotr, K. (A.P Instrument) 'Particle size analysis Zetasizer Nano Zetasizer Pro/Ultra', API Instrs [Preprint]. Available at: piotr.krystosiak@apinstruments.pl.

Richardson, S.H., Gurney, J.J., Erlank, A.J. and Harris, J., 1984. Origin of diamonds in old enriched mantle. Nature, 310(5974), pp.198-202.

Simakov, S.K., 2006. Redox state of eclogites and peridotites from sub-cratonic upper mantle and a connection with diamond genesis. Contributions to Mineralogy and Petrology, 151(3), pp.282-296.

Shakun, A., Vuorinen, J., Hoikkanen, M., Poikelispää, M. and Das, A., 2014. Hard nanodiamonds in soft rubbers: Past, present and future–A review. Composites Part A: Applied science and manufacturing, 64, pp.49-69.

Shigley, J.E., Chapman, J. and Ellison, R.K., 2001. Discovery and mining of the Argyle diamond deposit, Australia. Gems & Gemology, 37(1), pp.26-41.

Shimizu, Y., 2003. The nature of Ogasawara and its conservation. *GLOBAL ENVIRONMENTAL RESEARCH-ENGLISH EDITION*-, *7*(1), pp.3-14.

Tamil Many K Thandavan et al. 2010 'Diamond: Synthesis, Characterisation and Applications', p. 24.

Thandavan, Tamil Many K., et al. 2014 "Photoluminescence properties of un-doped and Mn-doped ZnO nanostructures." Materials Express 4.6: 475-482.

Trull, T., Nadeau, S., Pineau, F., Polve, M. and Javoy, M., 1993. C-He systematics in hotspot xenoliths: Implications for mantle carbon contents and carbon recycling. *Earth and Planetary Science Letters*, *118*(1-4), pp.43-64.

Thomas Stachel 2014 'Diamond', T. Stachel Department of Earth and Atmospheric Sciences University of Alberta, 1-26 Earth Sciences Building Edmonton, Alberta, p. 29.

Trull, T., Nadeau, S., Pineau, F., Polve, M. and Javoy, M., 1993. C-He systematics in hotspot xenoliths: Implications for mantle carbon contents and carbon recycling. Earth and Planetary Science Letters, 118(1-4), pp.43-64.

Wild, C., Koidl, P., Müller-Sebert, W., Walcher, H., Kohl, R., Herres, N., Locher, R., Samlenski, R. and Brenn, R., 1993. Chemical vapour deposition and characterization of smooth {100}-faceted diamond films. Diamond and Related Materials, 2(2-4), pp.158-168.

List of Figures

List of Tables

List of Equations